Article

Coastal Erosion Identification and Monitoring in the Patras Gulf (Greece) Using Multi-Discipline Approaches

Nikolaos Depountis [1,*], Dionysios Apostolopoulos [1], Vasileios Boumpoulis [1], Dimitris Christodoulou [1], Athanassios Dimas [2], Elias Fakiris [1], Georgios Leftheriotis [2], Alexandros Menegatos [1], Konstantinos Nikolakopoulos [1], George Papatheodorou [1] and Nikolaos Sabatakakis [1]

[1]   Department of Geology, University of Patras, 26504 Patras, Greece
[2]   Department of Civil Engineering, University of Patras, 26504 Patras, Greece
*   Correspondence: ndepountis@upatras.gr

Abstract: The primary objective of this research is to demonstrate advanced surveying methods and techniques for coastal erosion identification and monitoring in a densely human-populated coastline, the southern coastline of the Gulf of Patras (Greece), which diachronically suffers erosion problems expected to become worse in the forthcoming years due to climate change and human intervention. Its importance lies in the fact that it presents a robust methodology on how all modern scientific knowledge and techniques should be used in coastal erosion problems. The presented methods include the use of satellite and aerial photo imaging, shallow seabed bathymetry and morphology, sediment sampling, geotechnical investigations, as well as hydrodynamic modelling. The results are extensively analyzed in terms of their importance in coastal erosion studies and are cross-validated to define those areas most vulnerable to erosion. Towards this scope, the seabed erosion rate produced by hydrodynamic modelling is compared with the coastal vulnerability index (CVI) calculations performed in the examined area to identify which coastal zones are under a regime of intensive erosion. The results between the CVI and the seabed erosion rate appear to coincide in terms of the erosion potential, especially in zones where the vulnerability regime has been calculated as being high or very high, with the *P. oceanica* meadows playing an important role in reducing erosion.

Keywords: coastal erosion; coastal vulnerability index (CVI); geotechnics; remote sensing; marine survey; *P. oceanica*; hydrodynamic modelling; seabed erosion

1. Introduction

It is well known that climate change is causing adverse phenomena in both the terrestrial and marine environments. As a result, coastal erosion is expected to be increased shortly affecting a significant proportion of the human population [1], since demographic trends show that more and more people will be living in coastal risk-prone areas in the coming decades [2,3]. Among the others, the increasing impact of coastal flooding due to sea level rise [4–7] and climate change are very likely to affect the frequency and intensity of coastal disasters [3]. Coastal areas are also deteriorating from a variety of man-pressures connected with economic development and land use changes along the coastlines [8]. The resulting impacts of these climate-related and anthropogenic pressures will affect the ecosystems and generate socio-economic damages [4]. Therefore, important challenges arising and the future path includes enhanced climate projections and integration into impact models, impact assessments at a local scale, dynamic projections of spatially-distributed exposure and vulnerability, and exploration of inherently adaptive options [9].

In response to this situation, policy makers and designers are faced with the demanding task of preparing appropriate coastal management plans adapted to the climatic changes [9,10] and designing coastal adaptation strategies to tackle sea level rise [11]. Towards this goal, sophisticated tools must be applied to design the most appropriate

monitoring methods and numerical models for understanding erosion trends and designing solid infrastructures or nature-based measures. These tools range from index-based methods (e.g., coastal vulnerability index—CVI [12–14]) to decision support systems (DSS; e.g., DESYCO, DIVA, Theseus [15–17]), numerical simulations, and machine-learning approaches [18–20]. In any case, the initial step before the implementation of any method for erosion assessment is the understanding of coastal processes and mechanisms that exist in the coastal area through investigation and monitoring of the coastal zone and simulations of the relevant nearshore processes.

Specifically, monitoring of coastal zones is defined as a necessary procedure to collect, analyze, and store information about the morphodynamics and the processes that dominate and control coastal erosion [21], while it provides information on coastal changes due to storm events and human intervention [22]. Nowadays, long-term coastal erosion identification and monitoring are accomplished with multi-scientific on-site approaches that can provide quality data, accessible by the local and regional authorities for conducting scientific studies on coastal risks [23].These data may include measurements of the wave height, coastline changes, tidal range, currents, storm surges, and detection of shoreline position together with detailed marine remote sensing data (nearshore bathymetry and seabed morphology) [24].

Shoreline detection is usually performed with remote sensing techniques [25] such as aerial and satellite imagery [26–29] as well as Lidar applications [30–33]. In addition, unmanned surface vehicles (USVs) equipped with single-beam echo sounders, side scan sonars, and video cameras are used for the survey of nearshore bathymetry [34]. Another modern remote sensing technique is the detection of coastline position and bathymetry from video imagery, which has the advantage of obtaining information with high frequency in time [24,35–37].Unmanned aerial vehicles (UAVs) photogrammetry is used as well as an alternative tool to the acquisition of high-accuracy images along the littoral zone for shoreline monitoring [38]. Nowadays, the detection of the shoreline is mainly accomplished by image processing, while the evolution of remote sensing (RS), using high-resolution data has significantly reduced the margins of uncertainty providing results with great accuracy [39]. Many water indices can be applied, to delineate land from water, through their spectral bands [40], such as the normalized difference water index (NDWI) [41], improved from the modified NDWI [42], the normalized difference vegetation index (NDVI), and the automatic water extraction index (AWEI) [43]. Reviews of shoreline detection remote sensing techniques are presented in several studies [44–46].

Concerning the study of the bathymetry, morphology, and the substrate of the seabed of the shallow waters as well as the mapping of *Posidonia oceanica*, multibeam echo sounders, side scan sonars, and sub-bottom profilers are considered to be the most appropriate and sophisticated techniques [47]. *P. oceanica* is the dominant seagrass species in the shallow water environment of the Mediterranean Sea, which forms extensive prairies down to 35–40 m water depth [48,49]. These meadows are of crucial importance for the coastal environment since among others they buffer sediment resuspension, increase sediment retention [50], and stabilize the seabed, preventing sandy beach erosion [51].

Another important onshore and offshore surveying method is geotechnical surveying since a variety of technical projects are required to protect the anthropogenic and marine environment along the coastline. Therefore, the detection of geotechnical parameters in coastal sediments is a necessity in coastal erosion-accretion calculations, prediction of sediment transport and shear strength of seabed sediments [52], as well as for soil liquefaction assessment [53]. For this purpose, in situ geotechnical tests can be used to provide a potential relationship between the in situ data and the erodibility of seabed sediments [54]. Moreover, long-term subsurface sediment consolidation, settlement, and compressibility are predicted to provide coastal protection and resilience to future hazards [55]. Generally, the methodologies for calculating the rate of erosion and the critical shear strength are based on hydrodynamic theories or laboratory tests [56–59], but recently a conceptual framework based on a combined hydrodynamic and soil geotechnical approach for cohe-

sive beds which relates the erosion rate with the undrained shear strength of the soil has also been proposed [60]. Geotechnical surveys are also important to model coastal erosion, especially in coastal vulnerability index (CVI) calculations, either by adding geological strength indexes to estimate the quality of rocks against erosion [61] or by using specific geotechnical data [62].

Due to the development of computer technology and the growth registered in computational power, numerical modelling has also become increasingly popular in coastal research [63]. Nowadays, coastal hydrodynamic modelling is used for the prediction of nearshore processes, and it is a feasible approach to tackle issues such as coastal erosion and inundation. Furthermore, also taking into account the effect of climate change, coastal habitats are becoming increasingly vulnerable to erosion phenomena [64]. Thus, numerical modelling is a valuable tool to compute sediment transport rates, seabed morphological evolution and erosion rates in coastal zones, and to aid in the design of engineering measures/works for coastal defenses.

All the above-mentioned multi-discipline scientific approaches were combined for the first time, under the framework of the TRITON/Greece-Italy/Interreg V/A 2014-2020 co-operation project (2021), to examine and identify the coastal erosion of a densely human-populated area, the southern coastline of the Gulf of Patras in Greece. Among others, the project consists of two meaningful and distinct steps towards integrated coastal zone management (ICZM). The coastal erosion assessment step aims at the present-day evaluation of the erosion of the coastline and the identification of hot-spots areas of erosion. The observation step consists of the establishment of a regional observatory in combination with the real-time monitoring of several parameters to gain high value for modelling coastal hazards and many researchers mention it as a good practice for mitigation [23,65] and prediction of these threats [66–68]. Both steps are a necessity for the adequate design, construction, and maintenance of civil engineering coastal structures and the protection of the coastline against erosion.

In this context, the primary objective of the current research is to present identification and modelling techniques for coastal erosion problems (coastal erosion assessment step) using a robust methodological scheme consisting of multi-platform disciplinary approaches. For this purpose, advanced investigating methods for the efficient quantification of changes in coastal environments including satellite and aerial photo imaging, shallow seabed bathymetry, seabed morphology surveying, sediment sampling, and extensive geotechnical investigations are thoroughly presented and discussed. Moreover, results obtained from a hydrodynamic numerical model produced for the study area are presented along with the erosion rate of the seabed next to the coastline. Finally, the seabed erosion rate produced by the hydrodynamic modelling is compared with the coastal vulnerability index (CVI) calculations performed in the examined area to identify which coastal zones are under a regime of intensive erosion by also taking into account the *P. oceanica* meadows that generally inhibit erosion.

2. Study Area

The investigation area is located on the southern coastline of the Gulf of Patras (Western Greece) and extends to a total length of more than 40 km (Figure 1). It is a shallow embayment with a maximum water depth of about 120 m leading into the Ionian Sea on the west and the Gulf of Corinth on the east and its southern coastline receives deltaic sediment from the Peiros river.
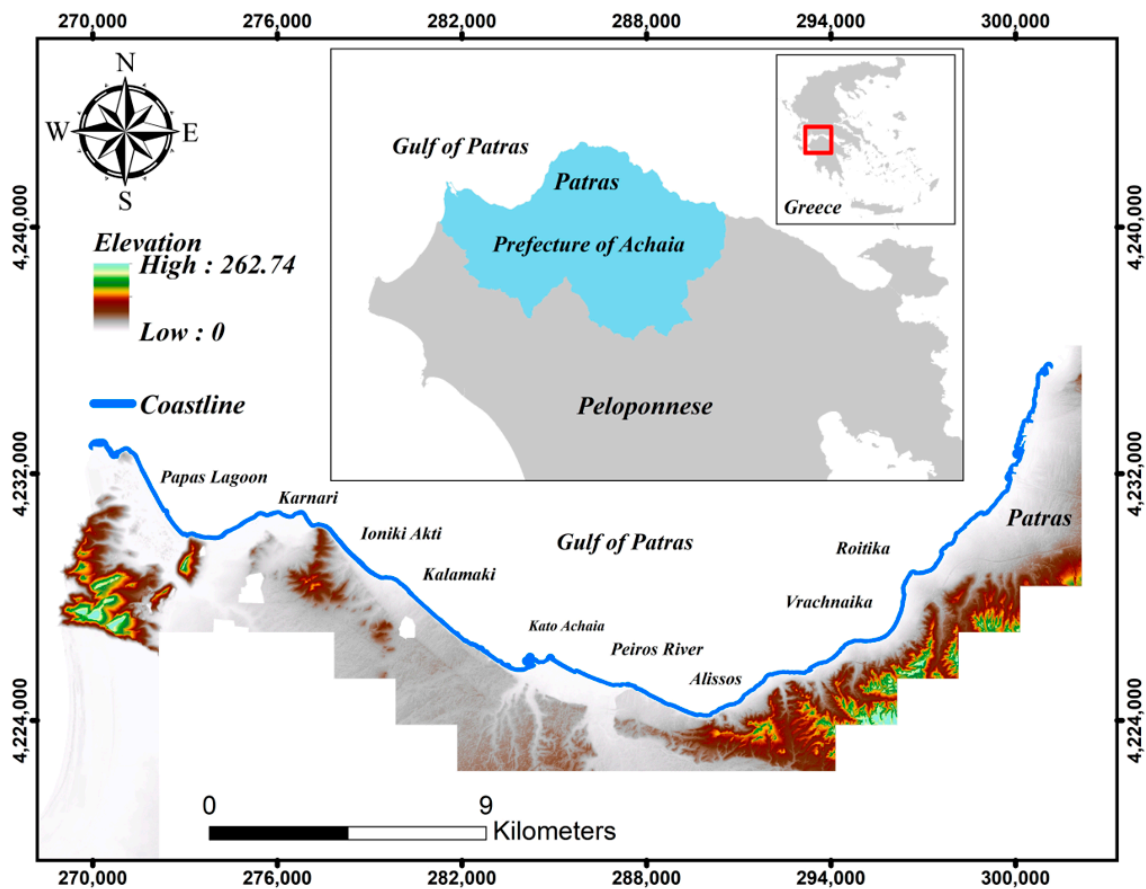
Figure 1. Map of the investigation area with the blue line representing the inspected south coastline of the Gulf of Patras. The geodetic coordinates of the map correspond to the Greek Geodetic Reference System—GGRS87.

The southern coastline of the Patras Gulf is a densely populated coastal zone, which suffers extensive erosion expected to become worse in the future not only due to climate change but also due to urban development and human intervention. The coastline can be divided into three sections. The northeastern section is densely populated and is heavily affected by the coastal constructions of the city of Patras. The central section of the coastline is controlled by the accretions of the Peiros river and on the western part the Pappas lagoon prevails (Figure 1).

3. Survey Design Plan for Coastal Erosion Identification

The TRITON project (2021) comprised a survey plan (Figure 2) consisting of (a) geotechnical surveys with drilling boreholes, in situ (CPT and SPT) and laboratory tests and sediment analyses for producing the necessary engineering geological base map with details on the prevailing coastal geotechnical units; (b) remote sensing surveys comprising satellite and aerial photo imaging accompanied with the use of UAVs to identify the historical shoreline movement for the last decades; (c) marine surveys, to identify the shallow seabed bathymetry and the seabed morphology for producing the relevant maps and to provide detailed oceanographic datasets; and (d) coastal engineering surveys for performing detailed hydrodynamic modelling; thus calculating the seabed erosion or accretion rate next to the coastline with the appropriate numerical simulations.
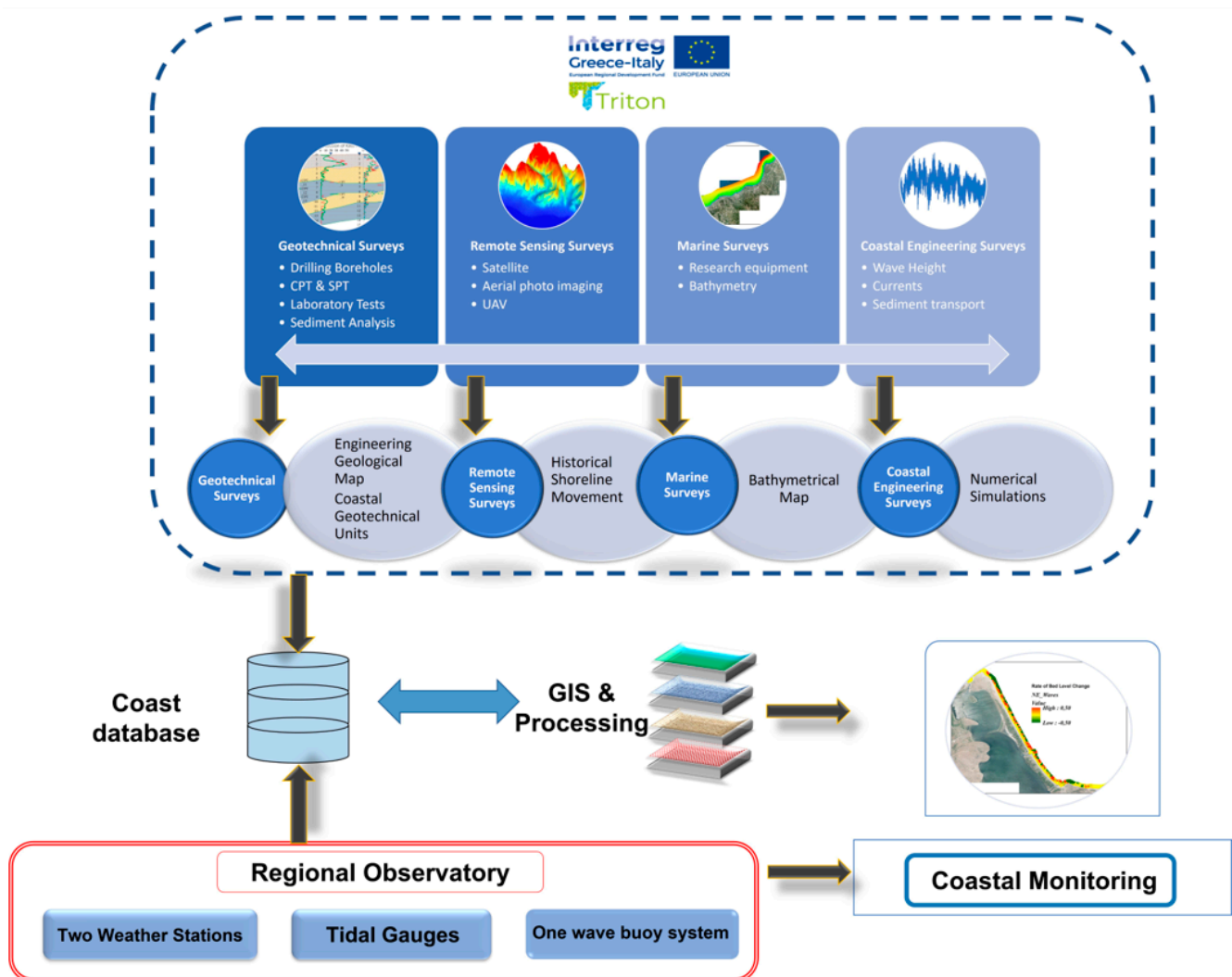
Figure 2. Survey design plan combined with a regional observatory for coastal monitoring of the suffered shoreline.

All data collected with the above-mentioned surveys were imported into a coastal database for further processing (GIS and numerical) to produce an accurate model of the affected area. However, this model needs continuous monitoring and real-data insertion; therefore, a coastal regional observatory had to be established to continually feed the database with all necessary information. For this purpose, a regional observatory consisting of (a) two weather stations, (b) two tidal gauges, and (c) one wave buoy system was established along the coastline of the Gulf of Patras. In this case the combination of surveying accompanied by the real-time data obtained from the observatory can be used in the coastal monitoring and the long-term protection of the affected shoreline (Figure 2).

3.1. Geotechnical Surveys

A detailed geotechnical research program was performed along the coastline of the study area, comprising of (a) the drilling of new and the collection of old marine and land boreholes (40 boreholes in total), (b) elaboration of in situ SPT and CPT tests, (c) performance of soil classification lab tests, and (d) sediment analysis from a total of one hundred and fifty-one (151) samples (Figure 3).
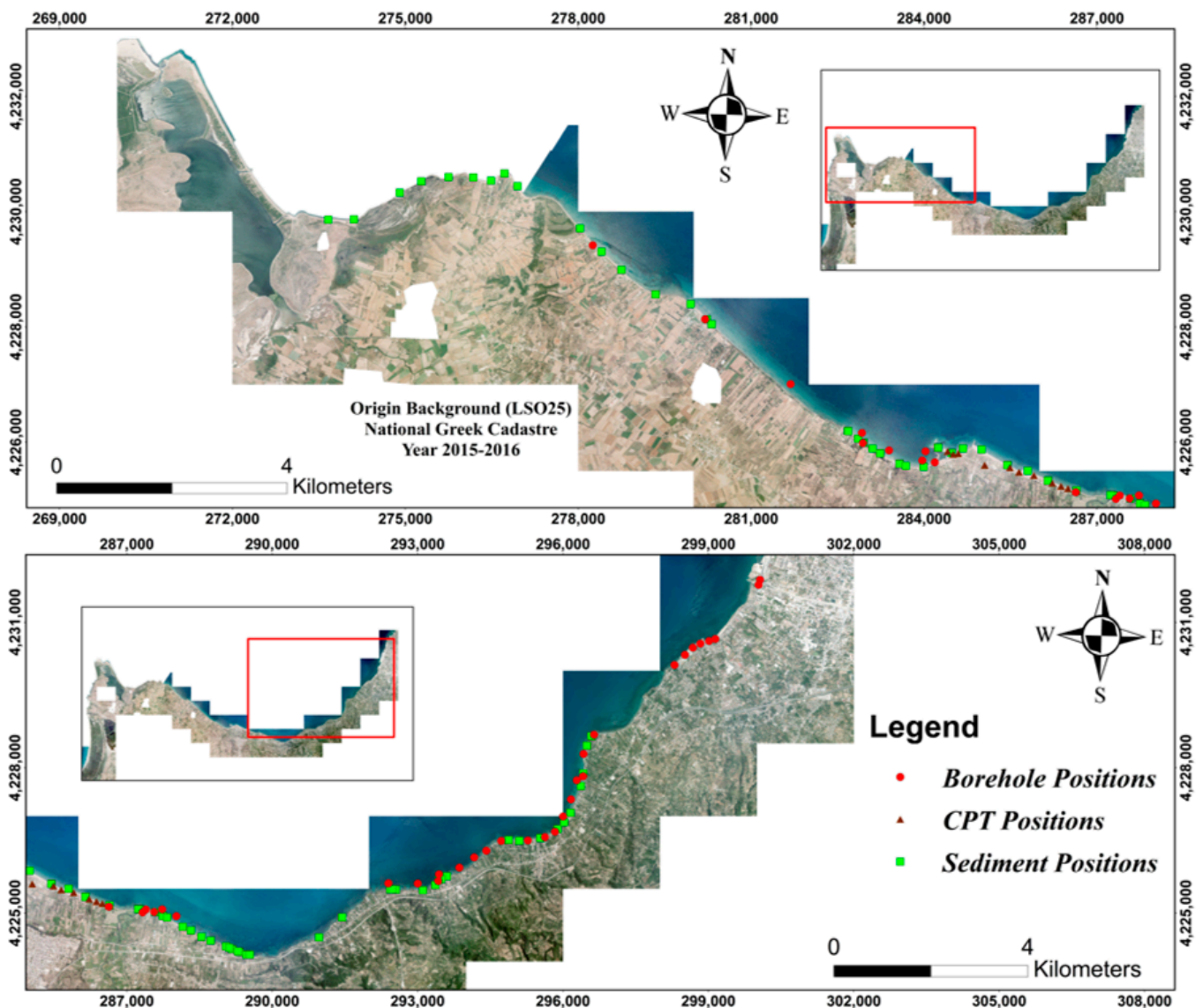
Figure 3. Map of the performed geotechnical surveys (borehole, CPT, and sediment sampling positions) along the south coastline of the Gulf of Patras.

By conducting this program, the soil's geotechnical behavior was identified, and a detailed engineering-geological map of the study area was designed to provide information for the CVI calculations and the hydrodynamic modelling that was performed in the current research.

3.2. Remote Sensing Surveys

Coasts are described as one of the most dynamic parts of the Earth's surface and have always been vulnerable to erosion and accretion fluctuations. Within the TRITON project (2021), the coastline evolution between Rion Port and Araxos Cape was recorded for the period 1987–2018 (Figure 4). For this purpose, remote sensing surveys were carried out and data were collected to estimate the rate of erosion for that period utilizing high-resolution images and photos and in situ measurements.
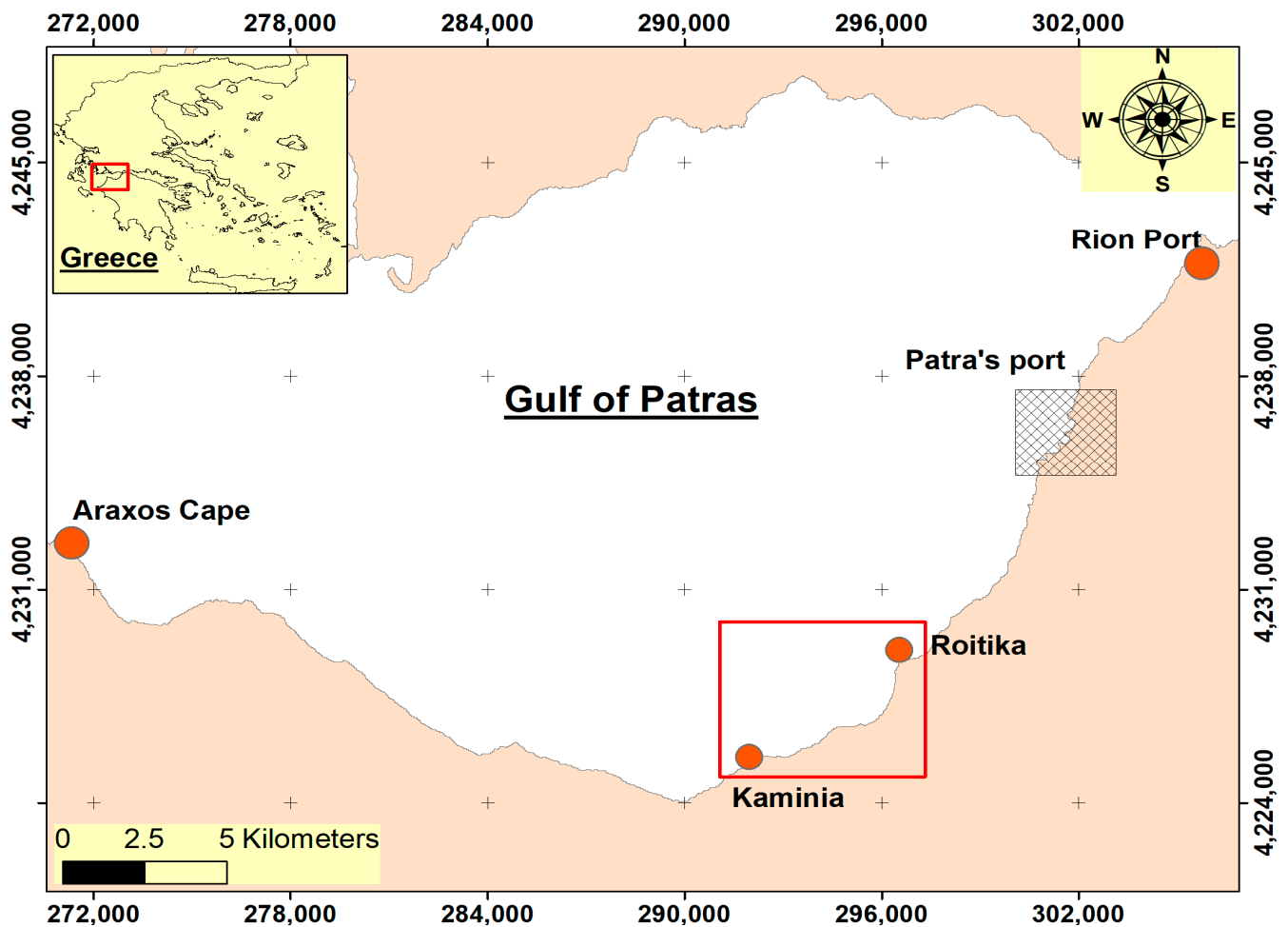
Figure 4. Study area (Araxos Cape–Rion Port) covered by the remote sensing datasets and test site (red frame area of Kaminia and Roitika villages) using GNSS measurements.

In detail, analogue aerial photographs collected at a scale of 1:30,000 (1987) were initially processed. The specific photos were scanned and orthorectified with a final pixel size of 1 m. Moreover, digital orthomosaics of 2008 and 2016 with a pixel size of 0.50 m and 0.25 m, respectively, as well as orthomosaics from the year 1996 with a pixel size of 1 m were also processed. In addition, a very high-resolution image of the Worldview-2 satellite with 50 cm spatial resolution, of September 2018, was processed in LPS. Orthomosaics of high-resolution airphotos and satellite images were processed using the Leica Photogrammetry Suite (LPS) of the ERDAS Imagine 2014 software.

To validate the results, and more specifically the erosion/accretion rates, GNSS measurements were also performed on the littoral area between Kaminia and Roitika villages in 2020 (Figure 4). It must be mentioned that Patras port was excluded from the measurements as it is an artificial area. The computing analysis of shoreline changes was finally performed using the Digital Shoreline Analysis System (DSAS) software [52].

Utilizing panchromatic and RGB orthomosaics, the shorelines were digitized based on the on-screen technique, as automatic methods are mainly generated based on spectral information provided by the bands of the images [69], and thus uncertainties and errors [70,71] were greatly reduced and limited to the pixel and rectification error. In addition, a baseline was manually drawn landward and parallel to the general shoreline orientation, while 50 m interval sections were digitized intersecting the baseline.

After that, the shoreline change was measured and compared for two periods, i.e., 1987–2018 and 1987–2020, computing the statistical rates such as the end point rate (EPR), and the net shoreline movement (NSM) provided by the DSAS software. The NSM

index, computes the range (m) between shorelines of different periods in each transect. The division of NSM value by time provides the EPR rate. Both of them may be negative or positive values [72,73]. After an almost excellent correlation of the rates of change for both periods in the test site, the shoreline movement was calculated for the entire study area (Araxos Cape–Rion Port) based on the remote sensing data for the 1987–2018 period.

3.3. Marine Survey: Fieldwork and Data Processing

For the bathymetry and the seabed morphology mapping of the shallow seafloor offshore of the southern coastline of the Gulf, multi/single beam echosounders (MBES, SBES) and side scan sonar (SSS) were used, respectively. The survey was carried out using the research vessel "Milady Millord III" (Figure 5a).
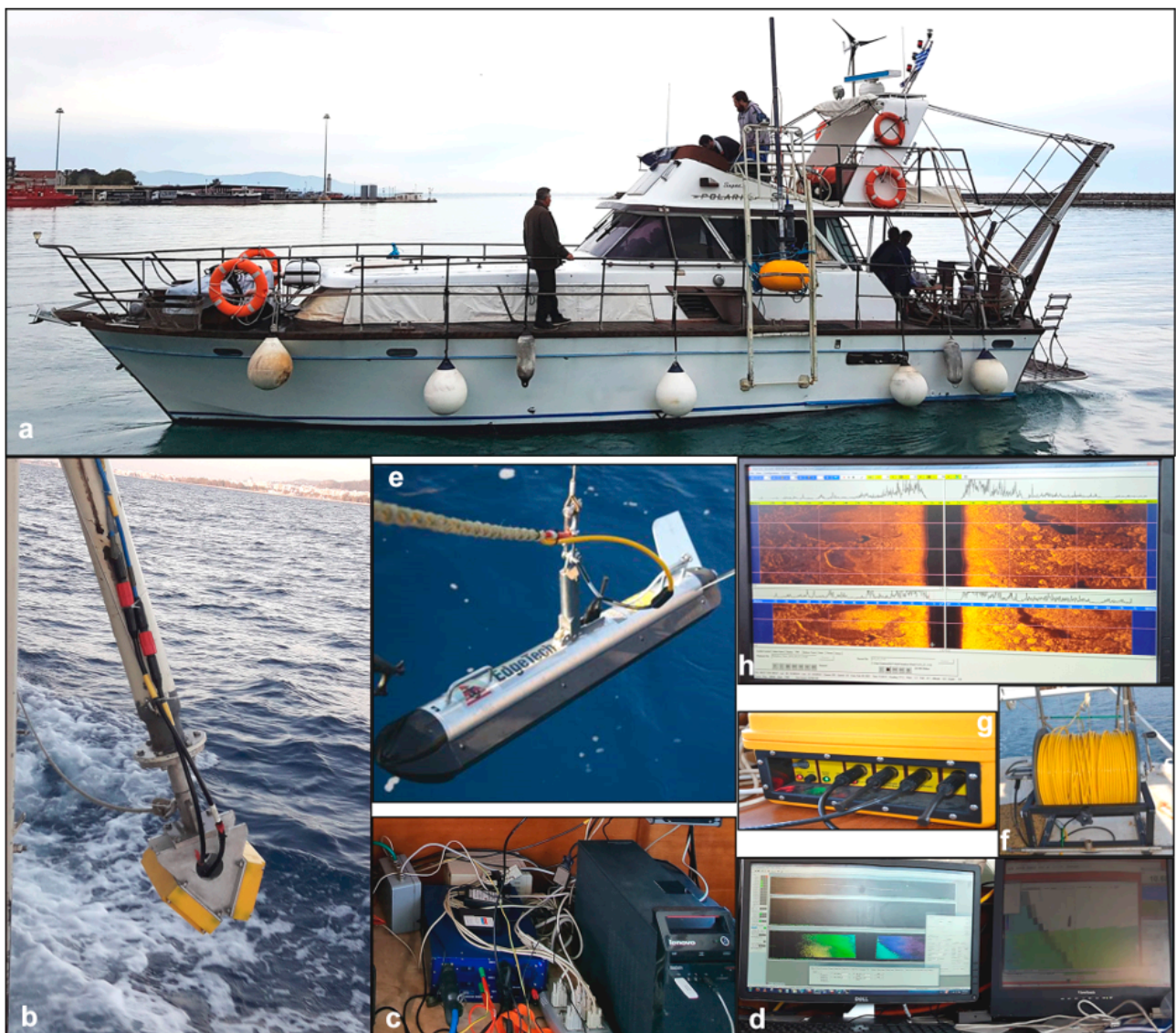
Figure 5. (**a**) The survey vessel "Milady Millord III", (**b**) Bathyswath1 transducers mounted over the side of the vessel, (**c**) Bathyswath1 Transmit/Receive Unit and operating workstation and (**d**) Bathyswath Swath Processor and Hypack 2010 during data acquisition, (**e**) Edgetech 4200 SSS Towfish, (**f**) SSS tow cable, (**g**) Edgetech 4200P digital recording unit, and (**h**) SSS data during acquisition.

3.3.1. Positioning—Navigation

For the position of the survey vessel a Differential Global Positioning System (DGPS) was used. The DGPS consists of: (i) a primary Leica GS08 GNSS System, which operated in RTK mode receiving corrections from the HEPOS (HEllenic POsitioning System) and (ii) a secondary Hemisphere VS101 GNSS System with an accuracy of ± 0.6 m 95% of the time. The research vessel navigation was carried out using the software package HYPACK 2014. The positioning of the geophysical equipment was also linked to HYPACK 2014. Moreover, for the multibeam bathymetric survey, a motion sensor (MRU) and a heading sensor were used for the continuous recording of the movements of the vessel.

3.3.2. Bathymetric Survey

The swath bathymetric sonar (interferometric sonar) BathySwath1 ITER System consisted of: (i) two transducers (Figure 5b) and (ii) a transmit/receive unit and a workstation (Figure 5c). BathySwath1 emits a wide swath width with a depth range from 0.2 to 100 m, offering resolutions as high as 2 cm. The bathymetric data were acquired using the Bathyswath Swath Processor and the HYPACK 2014 suite (Figure 5d). A Sea & Sun Technology Sound Velocity Profiler with a resolution of 0.001 m/s and accuracy ± 0.02 m was used for collecting sound velocity profiles. Moreover, a Hydrolite-TM single beam echosounder was used as a duplicate system for the checking of the swathe system, having a depth accuracy of 1 cm/0.1% of the water depth. Processing of swath bathymetric sonar and single beam echosounder data was performed using the Hypack and Hysweep software [74].

3.3.3. Seabed Morphology Survey

An Edgetech 4200 SP side scan sonar (SSS) system simultaneously emitting 100 and 400 kHz was used for the seabed morphology survey. The SSS system consists of (i) the SSS Towfish (Figure 5e), (ii) a Kevlar cable with a length of 200 m (Figure 5f) for both towing and data transfer, and (iii) the Edgetech 4200P digital recording unit (Figure 5g,h). For the mosaicking of the raw SSS data, Sea View MOSAIC (Moga Software) was used. The radiometric compensation of the data included automatic gain correction and destriping filtering while the geometric compensation included slant range and layback corrections and navigational spike removal. The pixel resolution of the mosaic was 0.5 m. The SSS sonograph shows a two-dimensional representation of the seafloor in terms of reflectivity (backscatter) as a function of sea-floor morphology, sediment texture (grain size and compaction), seafloor roughness, and biological formations [75].

3.3.4. Marine Survey Lines Design

The survey tracklines were planned for full mapping of the seabed through bathymetric (MBES) and SSS data. The vessel tracklines carried out for the bathymetric and side scan sonar survey are shown in Figure 6 covering an area of about 30 km^2.

3.4. Coastal Engineering Surveys

The coastal engineering survey was implemented by performing several numerical simulations of the waves, wave-generated currents, non-cohesive sediment transport, and bed morphodynamic evolution using MIKE 21 numerical software [76,77]. Specifically, the spectral waves (SW) module was used for the simulation of wave propagation, and the flow model (FM) module was used for the simulation of the current generation, sediment transport, and bed morphodynamics. The data imported to perform these simulations were derived by the geotechnical survey (sediment sampling and granulometric analysis), the marine survey (bathymetry), and wind data from the nearest to the study area meteorological stations (wind direction, speed, and intensity).
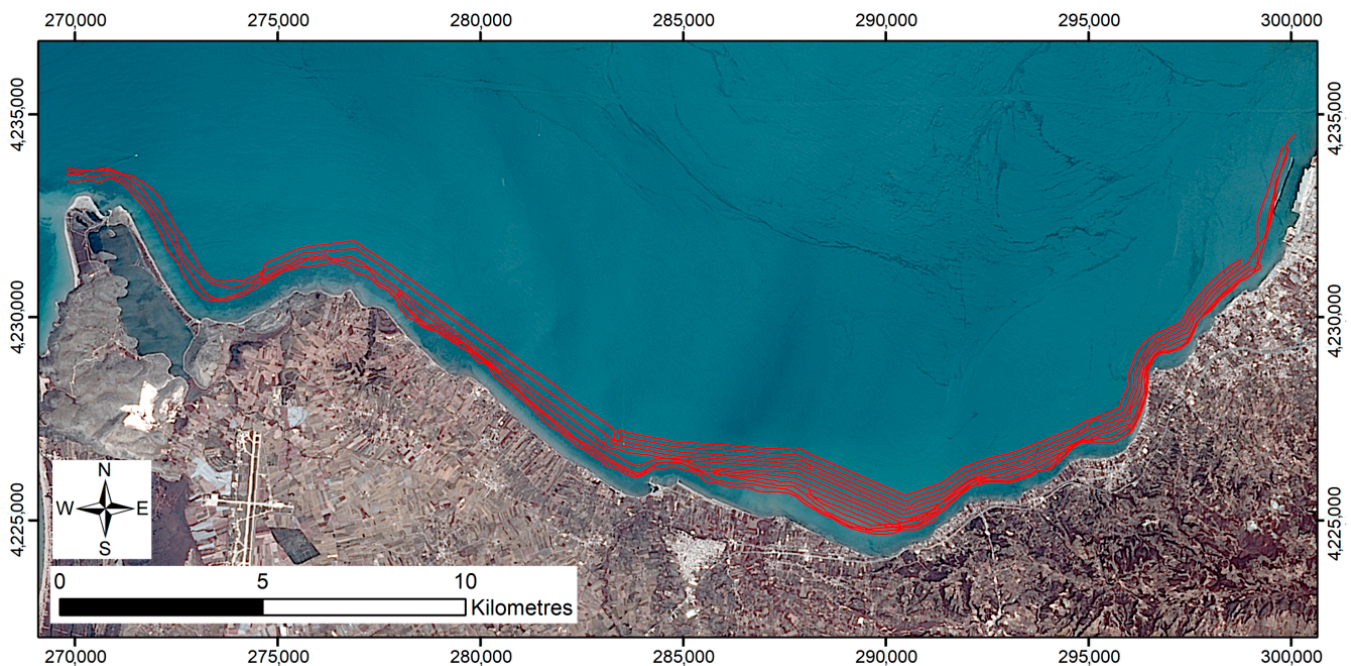
Figure 6. Map of the southern coastline of the Gulf of Patras showing the vessel tracklines.

The SW module can be used for the simulation of wind-induced wave generation, growth, and propagation, and includes a quadruplet-wave interaction model and a wave-breaking model [78]. The FM module includes the hydrodynamic part, which is based on the numerical solution of the shallow water equations and a formulation for the horizontal turbulent diffusion [79], and the sand transport part for the calculation of non-cohesive sediment transport and the resulting bed morphodynamic evolution.
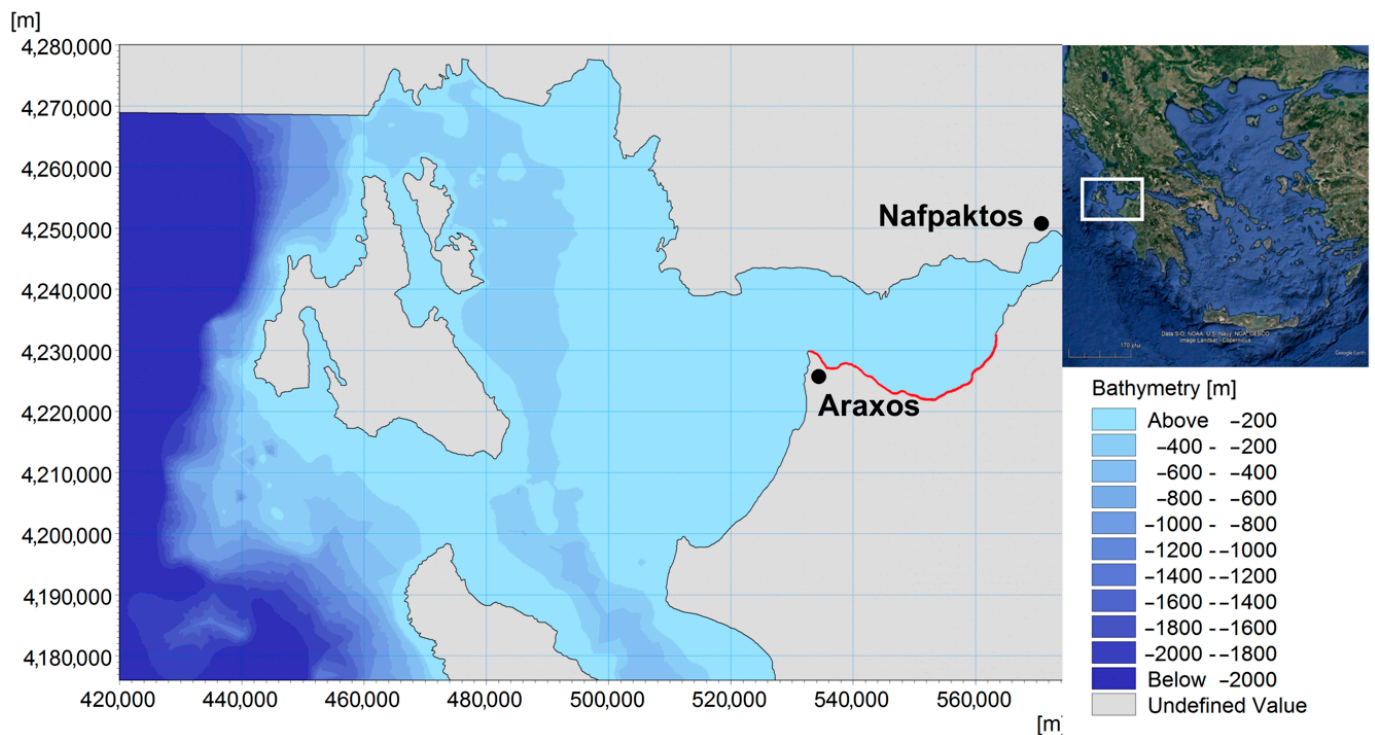
The numerical simulations comprise four stages:

- Determination of the deep-water wave parameters due to E, NE, NW, W, and SW winds in the study area.
- Nearshore wave propagation for wind speeds with a return period T_r = 1 year, for each wind direction.
- Nearshore numerical simulation of the magnitude and the direction of the wave-generated currents for each one of the wind cases of stage 2.
- Numerical simulation of the magnitude and the direction of sediment transport and bed morphodynamic evolution for each one of the wind cases of stage 2.

In stage 1, wind data from the Hellenic National Meteorological Service (HNMS) stations at the town of Nafpaktos (from 1/1/1977 to 31/12/2011) and Araxos Cape (from 1/1/1955 to 31/12/2011) were used to obtain the wind speed, U_{10}, with T_r = 1 year, for each wind direction, as presented in Table 1. Then, numerical simulations of wind-induced wave generation, growth, and propagation were performed using the SW module [77]. Apart from the wind data, input to the SW module is also the bathymetry of the computational domain, which includes the study area and part of the Ionian Sea between the islands of Kefallonia and Zakynthos (Figure 7). The computational domain was discretized with 181,406 triangular cells in an unstructured mesh with a resolution from about 100 m in shallow waters to about 300 m in deep waters. All the results are presented in Table 1.

In stage 2, numerical simulations of wave propagation and breaking were performed using the SW module [77]. Input to the SW module is the bathymetry of the southern coastal zone of the Gulf, and the wave characteristics at the offshore boundary as computed in stage 1. The computational domain was discretized with 189,936 triangular cells in an unstructured mesh with a resolution from about 100 m at the offshore boundary to about 10 m at the coastline. Results of the wave height and direction distribution in the southern coastal zone of the Gulf were obtained for all wind directions.

Table 1. Wind and wave data with T_r = 1 year, for each wind direction, calculated with the use of the data provided by the nearest to the study area meteorological stations.

| HNMS Station		Nafpaktos		Araxos		
Wind Direction		NE	E	NW	W	SW
Wind Speed, U_{10}	m/s	18.9	10.3	9.3	13.0	11.6
Wind Intensity	Beaufort	8	5	5	6	6
Significant Wave Height, $H_{S\text{-}1yr}$	m	2.7	0.6	0.6	1.8	1.5
Wave Spectrum Peak Period, $T_{P\text{-}1yr}$	s	8	4.4	5	8	6.8
Wave Direction to the North	°	45	60	315	270	235

Figure 7. The bathymetry of the computational domain of the Gulf of Patras and part of the Ionian Sea used in the numerical simulations (stage 1) of wind-induced wave generation, growth, and propagation. The red line indicates the coastline of the study area, while the black points indicate the location of the meteorological stations at Nafpaktos and Araxos.

In stages 3–4, numerical simulations of wave-generated currents, sediment transport, and bed evolution were performed using the FM module [76]. Input to the FM module is the bathymetry of the computational domain of the southern coastal zone of the Gulf, the geometry of existing harbor works, the sediment composition in the coastal zone, as well as the wave characteristics as computed in stage 2. The computational domain discretization was the same as in stage 2.

The bathymetries used were obtained by the digital database DHI C-MAP and the respective analytical measurements (marine survey) that were performed in this study.

For better comprehension of the coastal processes, the southern shoreline of the Gulf was divided into eight coastal independent zones, which are shown in Figure 8.
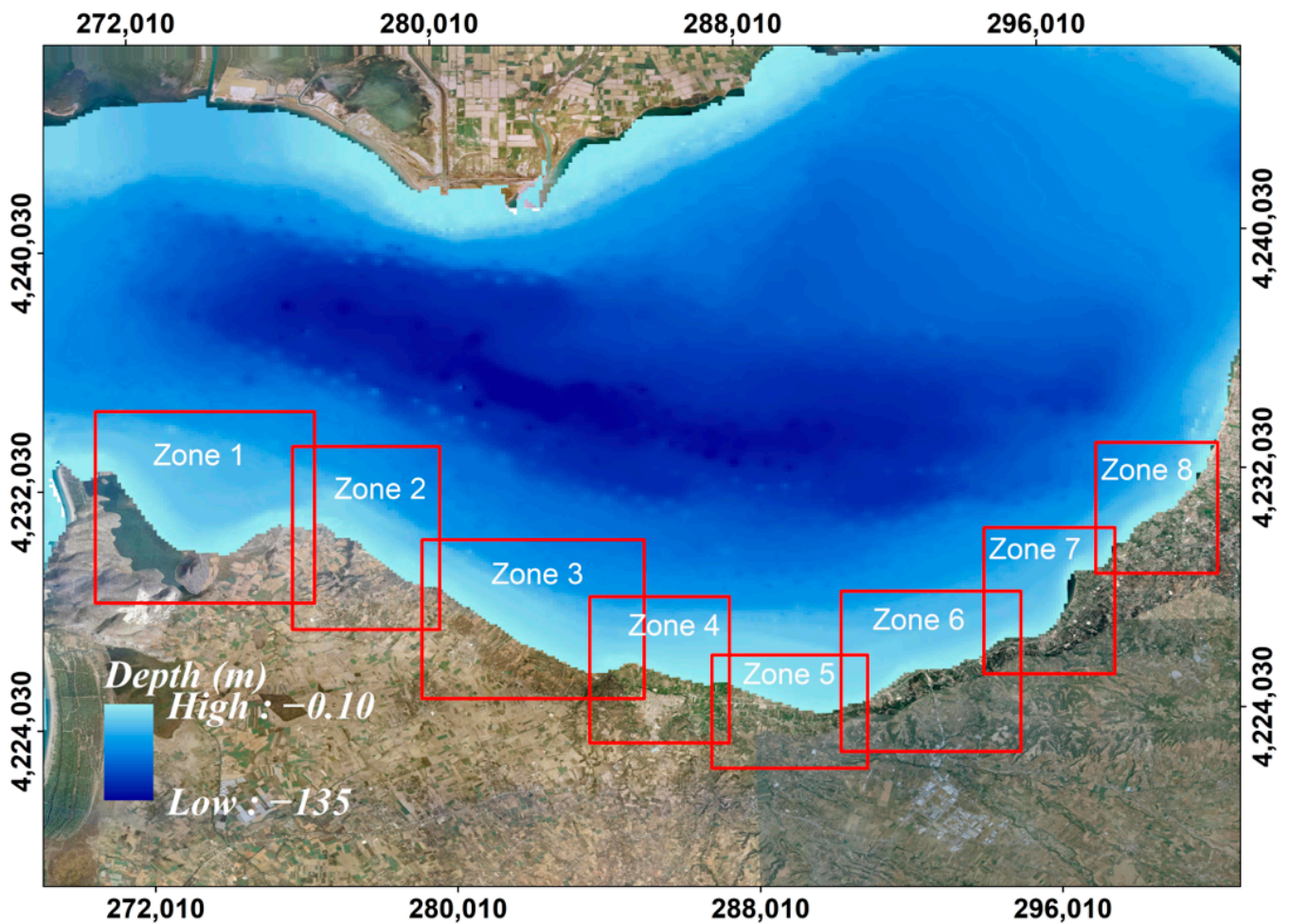
Figure 8. Map of the southern shoreline of the research area divided into 8 coastal independent zones, with the bathymetry used in the numerical simulations (stages 2, 3, and 4).

4. Results

4.1. Engineering Geological Map for Coastal Monitoring

Based on the field mapping, the laboratory and in situ tests, and the respective geotechnical evaluation, eight distinguished geological units were identified in a 1000 m zone parallel to the coastline of the study area (Figure 9).

(1) Coastal deposits (Sd): Sands, silty sands, and gravels of varying gradation, with characteristic diameter D_{50} = 0.67–3.97 mm

(2) Recent deposits (Q, c-l): Clayey sands of aeolian deposits and weatherings of older formations.

(3) Recent alluviums or torrential deposits (Qf, c-l): They consist of silt-clay, sands of various granulometric gradation, few gravels, and cobbles.

(4) River-lacustrine basin deposits (Qf, l): Clay and silt of river or lacustrine origin.

(5) Screes (Sc): Semi-cohesive screes with fine-grained materials.

(6) Pliocene–Pleistocene sediments (Pl, f-c): Yellowish to grey clays and marls, fine and medium-grained sands, brittle sandstones, and river-lacustrine and lagoon sediments.

(7) Flysch (Fl): Sandstones, siltstones, marls, and conglomerates.

(8) Limestones (Lm): Rock formation with thin layers of cherts.

As mentioned before, the engineering-geological map in Figure 9 was designed for specific coastal applications and infrastructure design purposes. Moreover, the coastal deposits (Sd) geotechnical unit of this map was further divided based on the geotechnical,

sedimentological, and morphological features of the area. The purpose was mainly to provide the necessary data for the later numerical modelling and to model the resistance to erosion parameter in the coastal vulnerability index (CVI) calculations that were performed after the completion of the TRITON project [62].
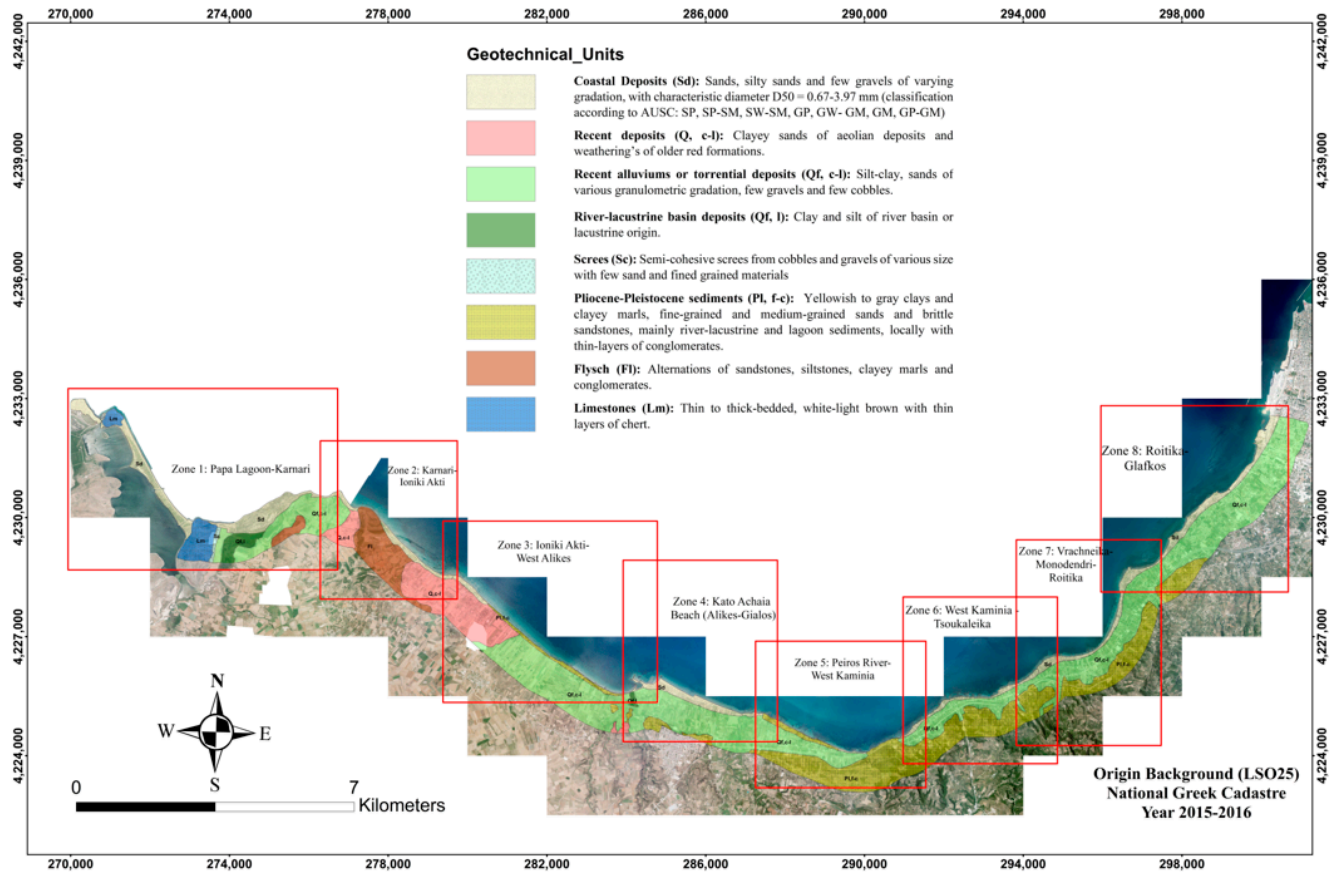

Figure 9. Engineering geological map with geotechnical units of the study area.

4.2. Orthomosaics and Aerial Photo Imaging Results

The EPR and the NSM models were applied to calculate the shoreline changes in the test area between Kaminia and Roitika villages. About 123 transects were cast on a total of 6 km of the tested littoral area. For the 1987–2018 period, the mean NSM rate was −7.02 m, and the max and min NSM values were +9.14 m and −21.12 m, respectively (Figure 10).
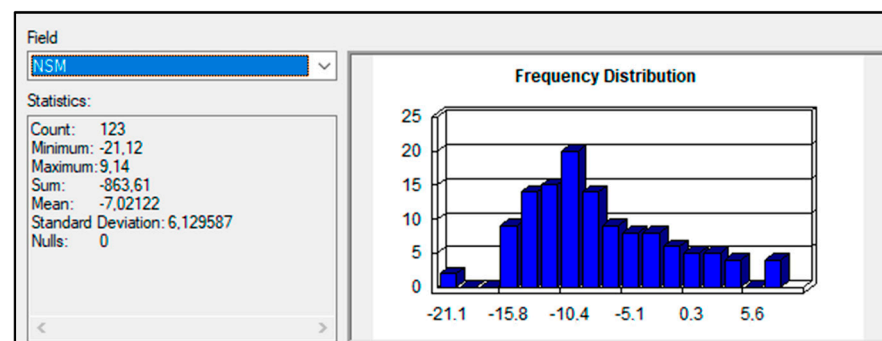

Figure 10. Statistical NSM rates for the 1987–2018 period between Kaminia and Roitika villages.

In Figure 11 the EPR (m/y) rates are presented for the 1987–2018 period for the same area. The minimum value is shown in red, while the maximum is shown in green,

corresponding to high erosion and accretion, respectively. Moderate erosion and accretion areas are represented with orange and light green, while values of stable areas ranging between −0.05 and +0.05 m/y are represented with blue. In the tested area, the maximum erosional degree was −0.68 m/y, whereas the maximum accretion reached +0.29 m/y. The mean rate of change was −0.22 m/y.
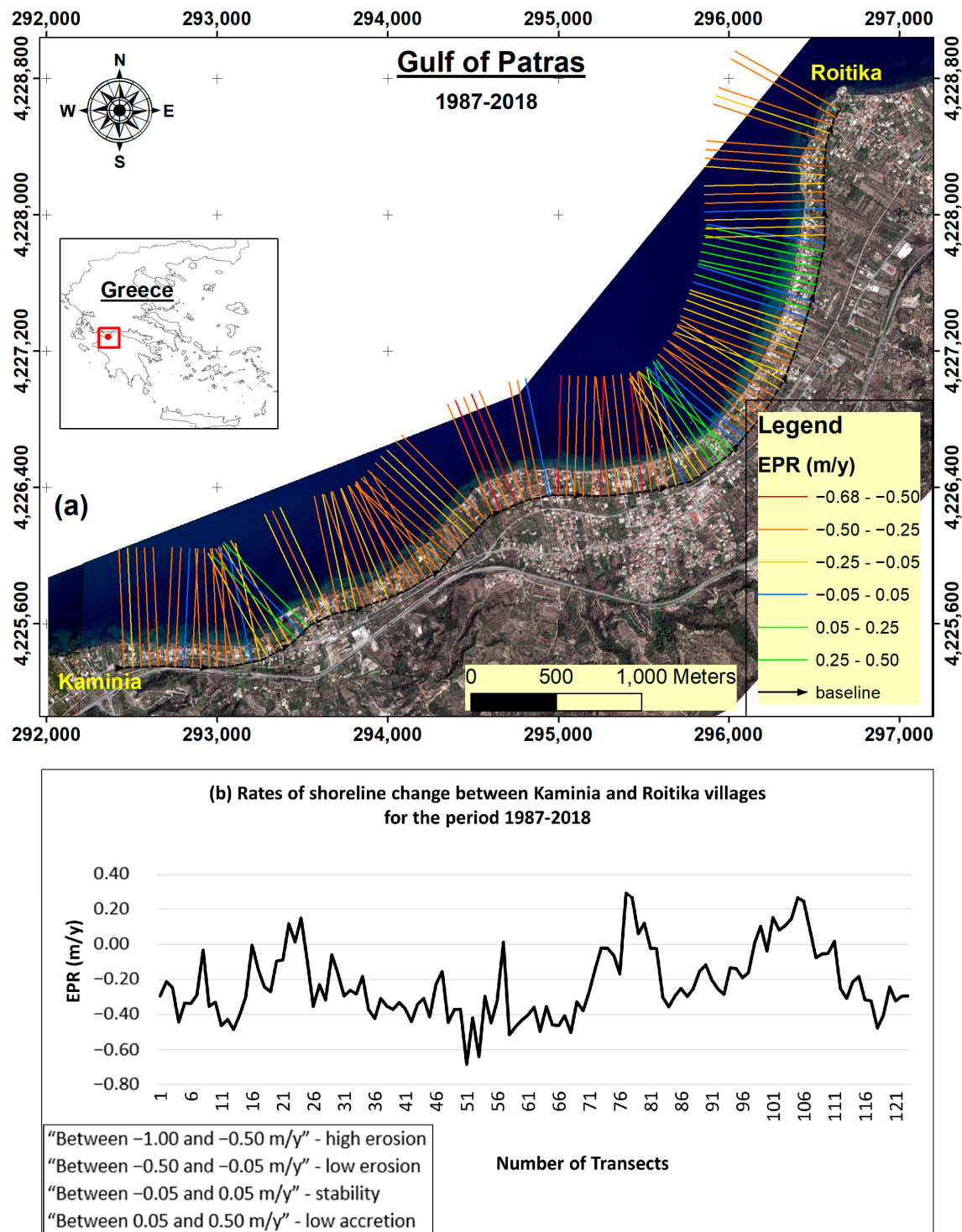
Figure 11. (**a**) Map showing the statistical EPR transects and (**b**) line graph showing the EPR values (mm/y) of each transect between Kaminia and Roitika villages for the period 1987–2018.

Furthermore, a topographic survey was made on December 2020 using a differential GPS receiver and 4240 points were taken along the entire length of the coastline of the test area. Those data were used to evaluate the measurements. The maximum rate of erosion and accretion for the 1987–2020 period was −0.61 m/y and +0.28 m/y and the mean value of change was measured at −0.24 m/y. As these rates, which correspond to the actual prevailing regime in the test area, were like those provided by the remote sensing techniques, the shoreline movement for the entire coast of the Gulf of Patras was finally calculated based on the remote sensing data for the 1987–2018 period.

In total, 995 transects were cast along the study area and after removing the outlier rates the remaining 824 were categorized into four classes associated with:

- high erosion "Between −1.00 and −0.50 m/y"
- low erosion "Between −0.50 and −0.05 m/y"
- stability "Between −0.05 and 0.05 m/y"
- low accretion "Between 0.05 and 0.50 m/y"

It emerged that the mean value of shoreline change was −0.21 m/y while the largest part (56%) of the study area, with a coast length of 28 km, was in a state of low erosion and 21% with a coast length of 10.5 km in a state of high erosion (Figure 12).
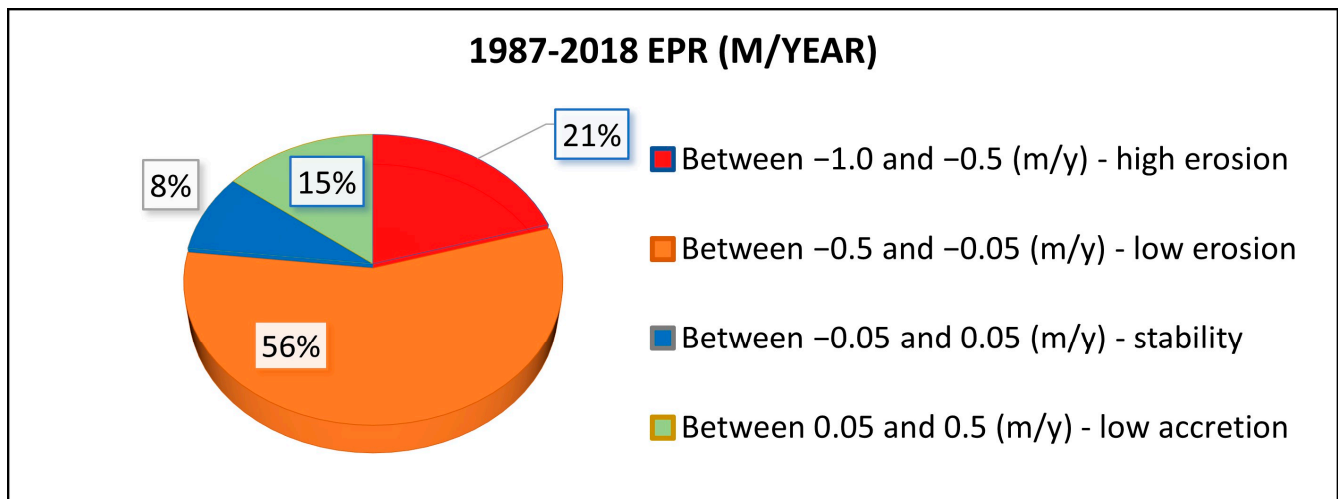

Figure 12. (%) State of erosion as part (%) of the study area according to the EPR rates (1987–2018).

4.3. Digital Bathymetric Plans and Results

The multibeam echosounder survey provided a detailed bathymetric map of the southern coasts of the Gulf of Patras down to 20 m water depth (Figure 13). Based on the bathymetric data and the seabed slope gradient, the seafloor in the survey area can be separated into five subareas (a–e).

The easternmost subarea (a) is characterized by high slope degrees (10°) between the 5 and 15 m isobaths and corresponds to zones 7 and 8 of Figure 8. The subarea (b) shows, locally, high degrees between the 5–10 m and 10–15 m isobaths and corresponds to zones 6 and 7 of Figure 8. The middle subarea (c) is characterized by very low slope degrees, with the lowest values obtained between the 5 and 15 m isobaths and corresponds to zones 4 and 5 of Figure 8. One notable exception, within the subarea (c), is the steep slope region offshore of the Kato Achaia promontory. Subarea (d) exhibits a moderate slope gradient (6–7°), locally, between the 5 and 20 m isobaths and corresponds to zones 2 and 3 of Figure 8. Finally high slope degrees are obtained in the westernmost subarea (e), between the 10 and 15 m isobaths, at the Araxos Cape corresponding to zone 1 of Figure 8.
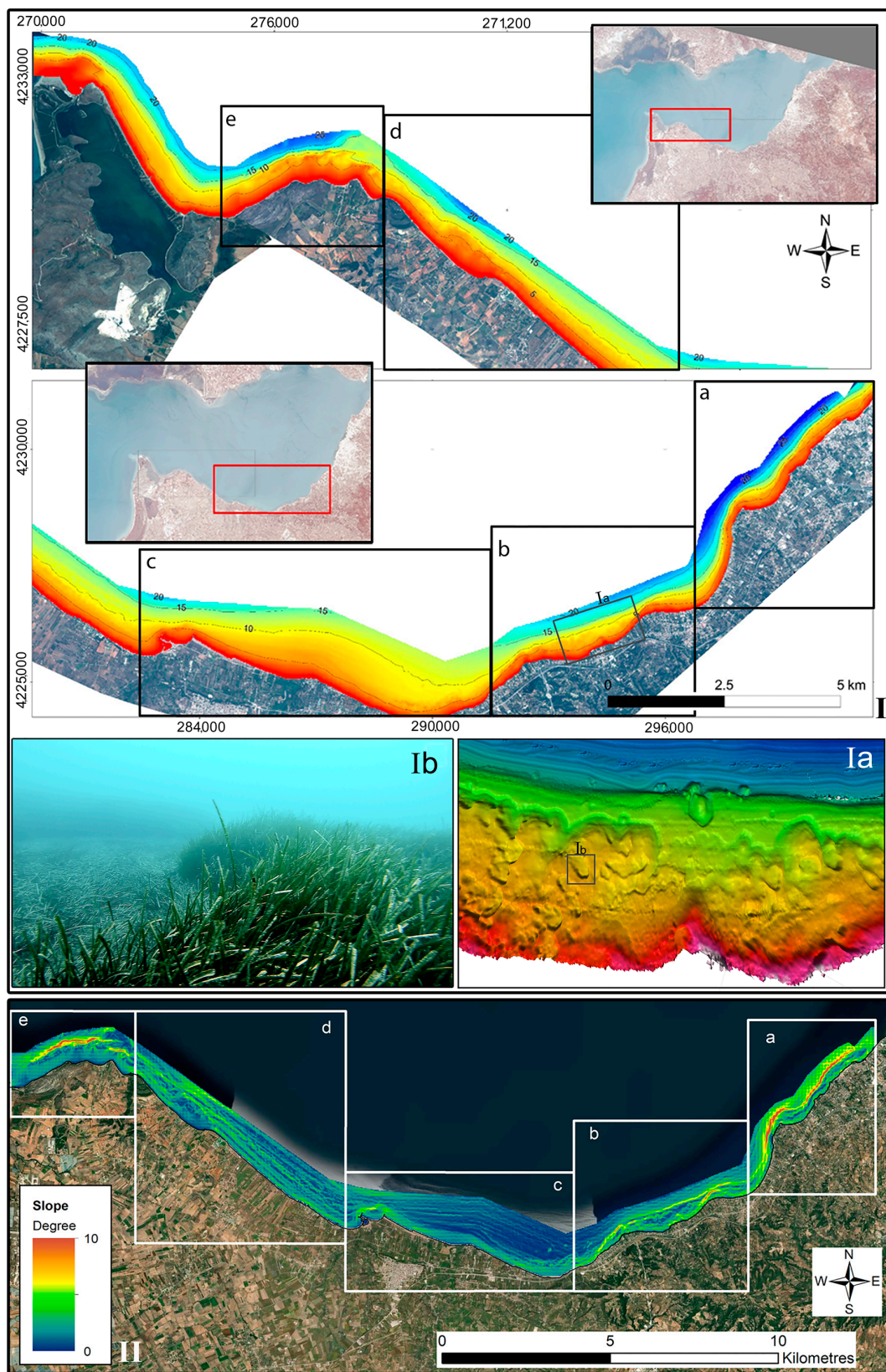
Figure 13. (**I**) Bathymetric map of the survey area. (**Ia**) Detailed bathymetry showing *P. oceanica* meadow morphology and (**Ib**) underwater photo of *P. oceanica*. (**II**) Slope gradient map of the survey area. Based on the multibeam bathymetric data and the slope gradient, the area has been separated into five (a–e) subareas.

The side scan sonar (SSSS) mosaics (Figure 14) and the local bathymetry revealed four distinct bottom classes, each one of distinct backscatter intensity, image texture, and morphology: (i) Fine sand: areas of low backscatter intensity with homogenous and low contrast image texture and low relief, covering a total area of 8 km^2 (34% of the survey area); (ii) coarse sand: areas of high backscatter intensity with homogenous and low contrast texture and low relief, covering a total area of 5.7 km^2 (24% of the survey area); (iii) *P. oceanica* meadows: high backscatter intensity areas with moderate texture variance and contrast (Figure 15) and high topographic ruggedness covering a total area of 8 km^2 (34% of the survey area); and (iv) sparse *P. oceanica* meadows: areas of moderate backscatter intensity with high texture variance and contrast, covering a total area of 2 km^2 (8% of the survey area).
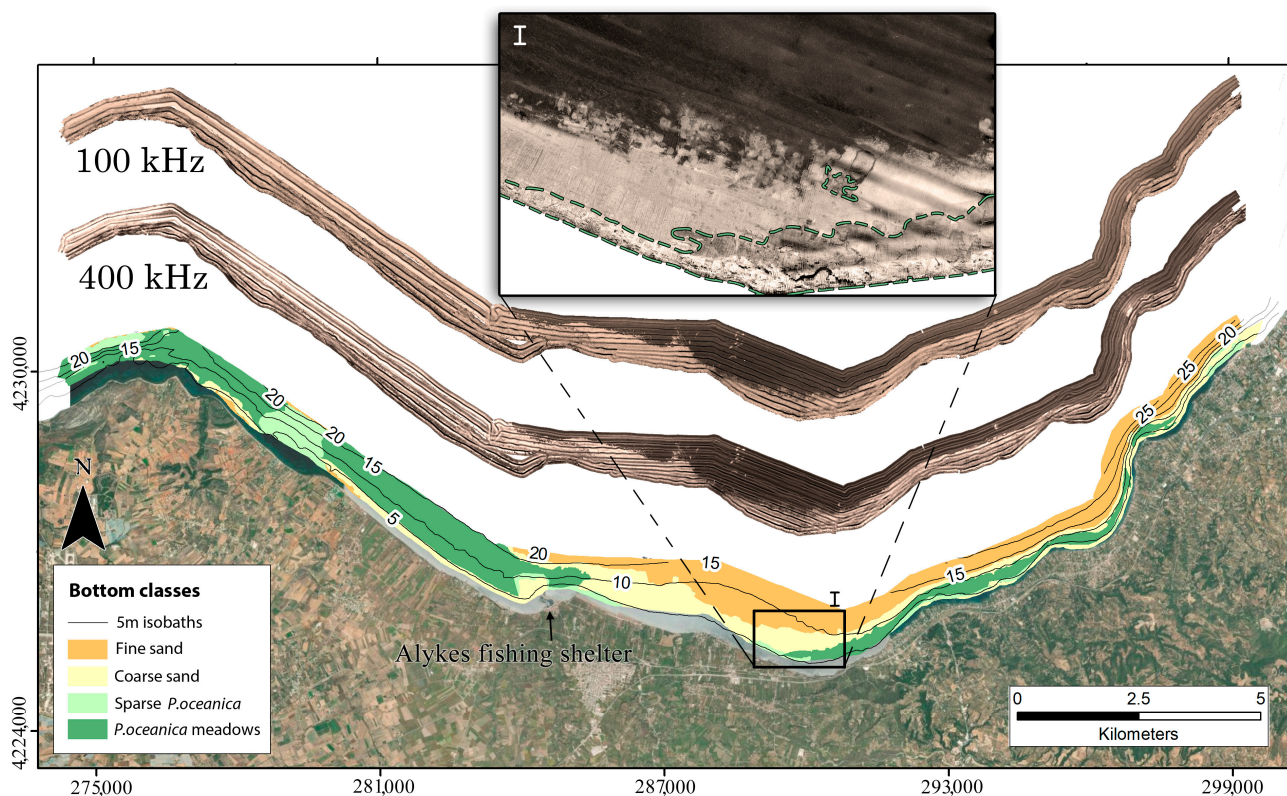
Figure 14. Seafloor map of the survey area showing four distinct bottom classes, based on the interpretation of the side scan sonar high (400 kHz) and low (100 kHz) frequency mosaics. (**I**) Corresponds to a mosaic detail including all bottom types, indicating with dashed line borders the areas classified as *P. oceanica* meadows.

P. oceanica beds prevailed in the surveyed area covering 42% (10 km^2) of the seafloor. The channels, which are filled with gas (aerenchyma) within the seagrass leaves, together with the gas bubbles produced during photosynthesis, are the dominant causes for the strong reflectivity (backscatter) of the seagrass meadows on the sonographs [55,56]. The shallower limits of *P. oceanica* classes are located at a water depth of about 5 m except for subareas –c- and –e- where the limit has been found shallower than 5 m. The deep limit is located deeper than 20 m in subareas –d- and –e- and shallower than 10 m in subareas –a-, –b-, and –c- (Figure 14).
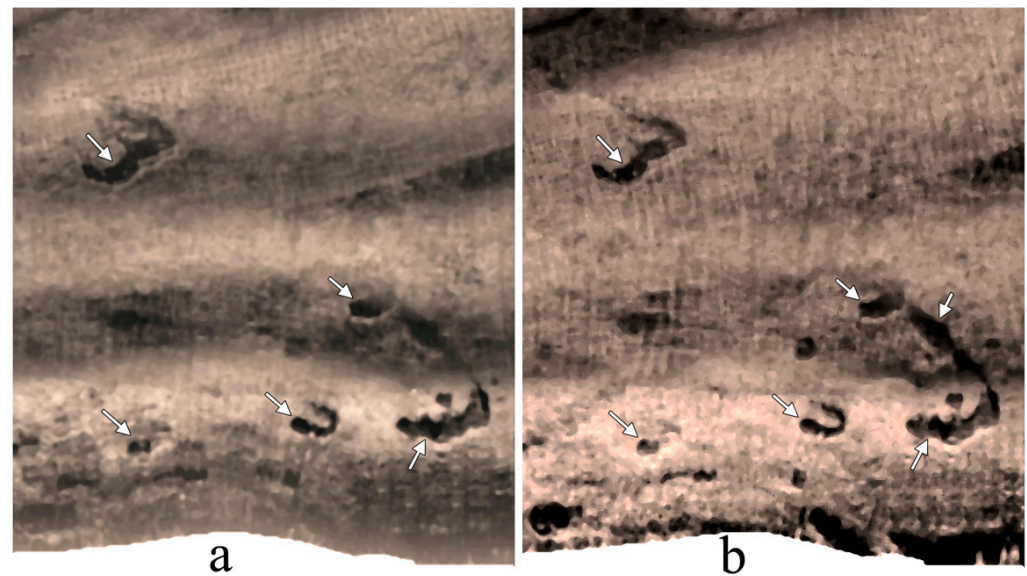
Figure 15. Sonograph of (**a**) 400 and (**b**) 100 kHz showing representative dense, almost continuous and uniform *P. oceanica* meadows. Arrows indicate sand gaps inside *P. oceanica* meadow.

In general, *P. oceanica* seagrass seems to be getting much more extensive to the west of Kato Achaia promontory (subareas –d- and –e- corresponding to zones 1, 2, and 3 of Figure 8), most likely due to: (i) having lower slopes and (ii) being further from any anthropogenic interference, such as industrial and recreational coastal activities and urban waste treatments. For instance, a major gap in *P. oceanica* spatial distribution, found between 21°33′ E and 21°36′ E in Figure 14, is directly related to the outlet river network of Peiros-Parapeiros whose sediment yield has been seriously affected by the construction of a dam south of the investigation area. The Peiros-Parapeiros river basin is mainly affected by agricultural, rural, municipal, and industrial activities, while the natural environment has been altered by the construction of the dam.

Other minor gaps are found around 21°32′ E, related to a beach groyne built eastwards of the Alykes fishing shelter causing sedimentation to its eastern side and eastwards 21°41′ E, where the urban wastewater sewage system of the city of Patras has been installed in combination with steep seabed slopes, not allowing the *P. oceanica* to flourish (Figure 14). These areas in which *P. oceanica* is almost absent correspond to zones 4, 5, and 8 of Figure 8.

4.4. Coastal Engineering Results

Based on the numerical simulations performed, several comments regarding the rate of the sea bed level change can be made for the entire investigation area.

The action of NE winds induces waves with large significant wave heights on the west coast of the study area, as well as intense wave-generated currents. As a result, intense coastal erosion (high rates of sea bed level change) is observed throughout zones 1, 2, and 4 (Figure 16). On the other hand, the action of NW and W winds creates favorable erosional conditions (high rates of sea bed level change) in zones 6, 7, and 8 along the southern coastal zone of the Gulf of Patras (Figure 16).

Table 2 summarizes the erosional intensity (sea bed level change) in the eight zones of the study area with respect to the wind direction.
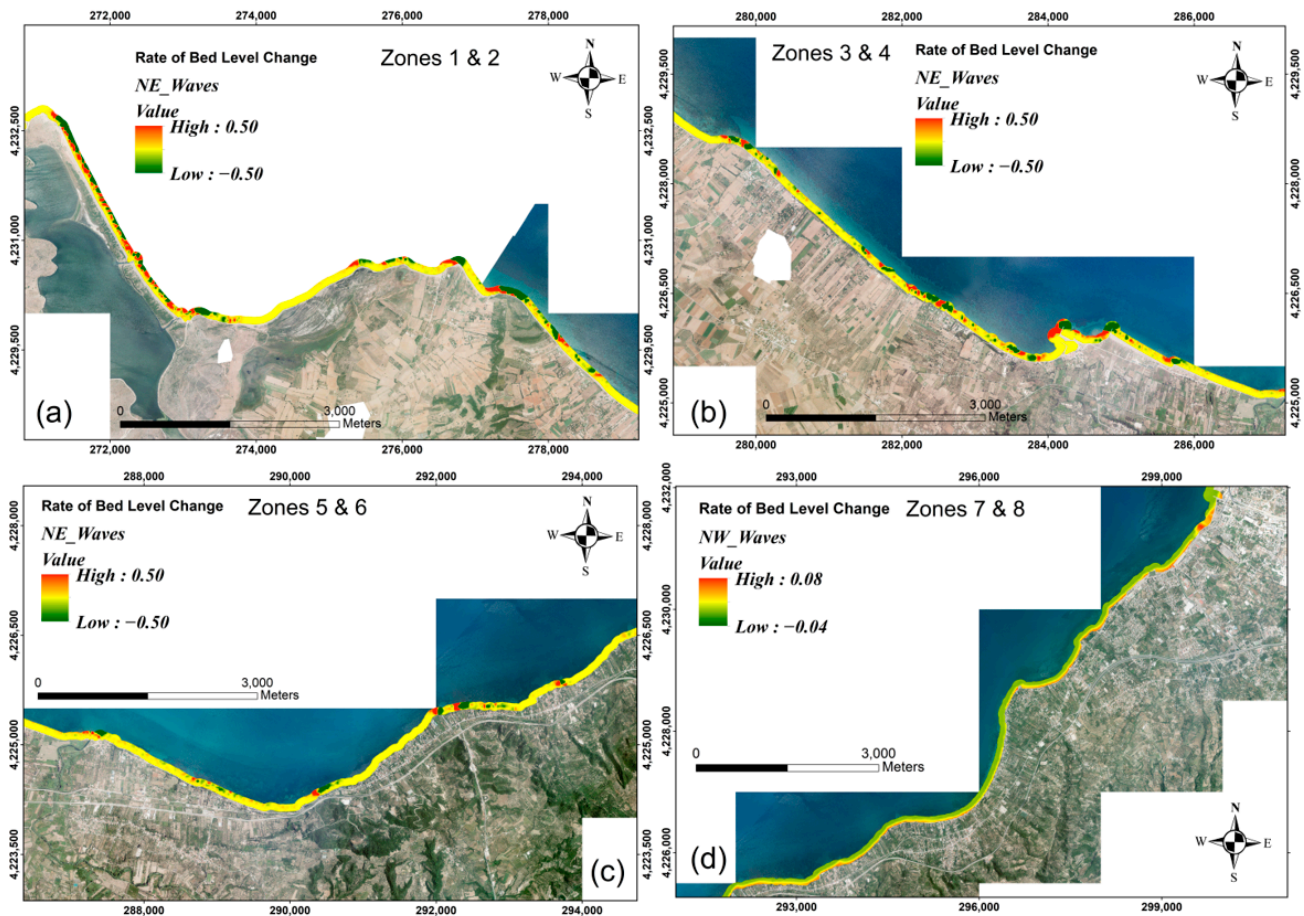
Figure 16. Seabed level change in (**a**) coastal zones 1 and 2, (**b**) zones 3 and 4, (**c**) zones 5 and 6 due to NE waves, and (**d**) coastal zones 7 and 8 due to NW waves. These are the most affected sea bed level change winds in the respective areas.

Table 2. Erosional intensity in the 8 zones of the study area with respect to the wind direction.

	Zone	NE	NW	W	SW
1	Papas Lagoon-Karnari	High	Low	Null	Null
2	Karnari-Ioniki Akti	High	Low	Null	Null
3	Ioniki Akti-Alykes	Moderate	Low	Null	Null
4	Alykes-Gialos (Peiros estuary)	High	Low	Null	Null
5	Gialos-Western Kaminia	Moderate	Moderate	Low	Null
6	Western Kaminia-Western Vrachneika	Moderate	High	Moderate	Null
7	Western Vrachneika-Roitika	Low	High	High	Null
8	Roitika-Glafkos	Null	High	High	Null

4.5. Coastal Vulnerability Index (CVI)

After the completion of the TRITON project, the vulnerability to coastal erosion along the southern coastline of the Gulf of Patras was ascertained by performing CVI calculations. The overall CVI consists of six parameters; (i) shoreline change rates, (ii) significant wave height, (iii) tidal range, (iv) coastal slope/relief, (v) relative sea level, and (vi) geomorphology and geology. For the accurate estimation of the geological and geomorphological parameter, special emphasis has been placed on the geotechnical characteristics of the survey area. Based on that, a new modified CVI_{WF} model was suggested by replacing the geological and geomorphological parameter with the geotechnical parameter as it was indicated in the current research [62]. The results of the dimensional analysis from the

CVI$_{WF}$ model disclosed that zones 1, 4, 7, and 8 have a high vulnerability, zone 2 has a low to moderate vulnerability, zones 5 and 6 have a low vulnerability, and zone 3 has a very low vulnerability [62]. The results of the calculated CVI$_{WF}$ compared with the erosional intensity per wind direction in the area of interest are presented in Table 3.

Table 3. Results of the CVI$_{WF}$ compared with erosional intensity per wind direction.

|	Zone	Erosional Intensity Per Wind Direction	CVI$_{WF}$ Vulnerability Class
1	Papas Lagoon-Karnari	High/NE	High
2	Karnari-Ioniki Akti	High/NE	Low-Moderate
3	Ioniki Akti-Alykes	Moderate/NE	Very Low
4	Alykes-Gialos (Peiros estuary)	High/NE	High
5	Gialos-Western Kaminia	Moderate/NE	Low
6	Western Kaminia-Western Vrachneika	High/NW	Low
7	Western Vrachneika-Roitika	High/NW	High
8	Roitika-Glafkos	High/NW	High

5. Discussion

The aim of this research is to demonstrate advanced surveying methods and techniques for coastal erosion identification and monitoring. For this purpose, geotechnical investigations, sediment sampling, satellite and aerial photo imaging, bathymetric surveys, as well as hydrodynamic modelling were utilized for the identification of the erosion status and trend along the southern coastline of the Gulf, which was selected as a test (pilot) area due to its timeless erosion problems and its economic importance to the local community. Furthermore, all the survey data were imported into a coastal database for various processing to produce an accurate model of the affected area.

The hydrodynamic numerical model produced from this process was used to estimate the erosion rate of the seabed next to the coastline. Additionally, a CVI$_{WF}$ calculation was performed to identify the vulnerability to coastal erosion.

Finally, a complete image of the CVI$_{WF}$ spatial distribution together with the bed level change under the two prevailing wave directions (NW and NE waves) and the *P. oceanica* meadows coverage was produced and is presented in Figure 17 for further discussion.

Comparing the results of the erosion intensity next to the coastline (bed level change) with the calculated CVI$_{WF}$, it seems that they partially agree, especially in areas where the vulnerability regime was calculated as high or very high. These areas are (i) zone 1 (Papas lagoon–Karnari), (ii) zone 4 (Alykes–Gialos, Kato Achaia), zone 7 (Western Vrachneika–Roitika), and zone 8 (Roitika–Glafkos).

Concerning the *P. oceanica* meadows, it is well known that they play a crucial role in coastal protection, by stabilizing the coastline, controlling beach morphology, and reducing wave energy [50,51]. Although the CVI$_{WF}$ does not consider those positive effects of *P. oceanica* meadows on coastal protection, a comparison of their spatial distribution may be of interest. The comparison of the spatial distribution of the *P. oceanica* meadows with the vulnerability class showed that: (i) the absence of meadows are related with the high to very high vulnerability of zone 4 (Alykes–Gialos, Kato Achaia) and zone 8 (Roitika–Glafkos), (ii) the very narrow and sparse meadows are linked with the high vulnerability of zones 6 (western Kaminia–western Vrachneika), and 7 (Western Vrachneika–Roitika), (iii) the well-developed and wide meadows at zones 1, 2, and 3 seem to have a positive effect of the vulnerability of the shoreline with the exception of two areas (Karnari and Kalamaki) where the high CVI$_{WF}$ corresponds to limited areas of sparse meadows (Figures 14 and 17).
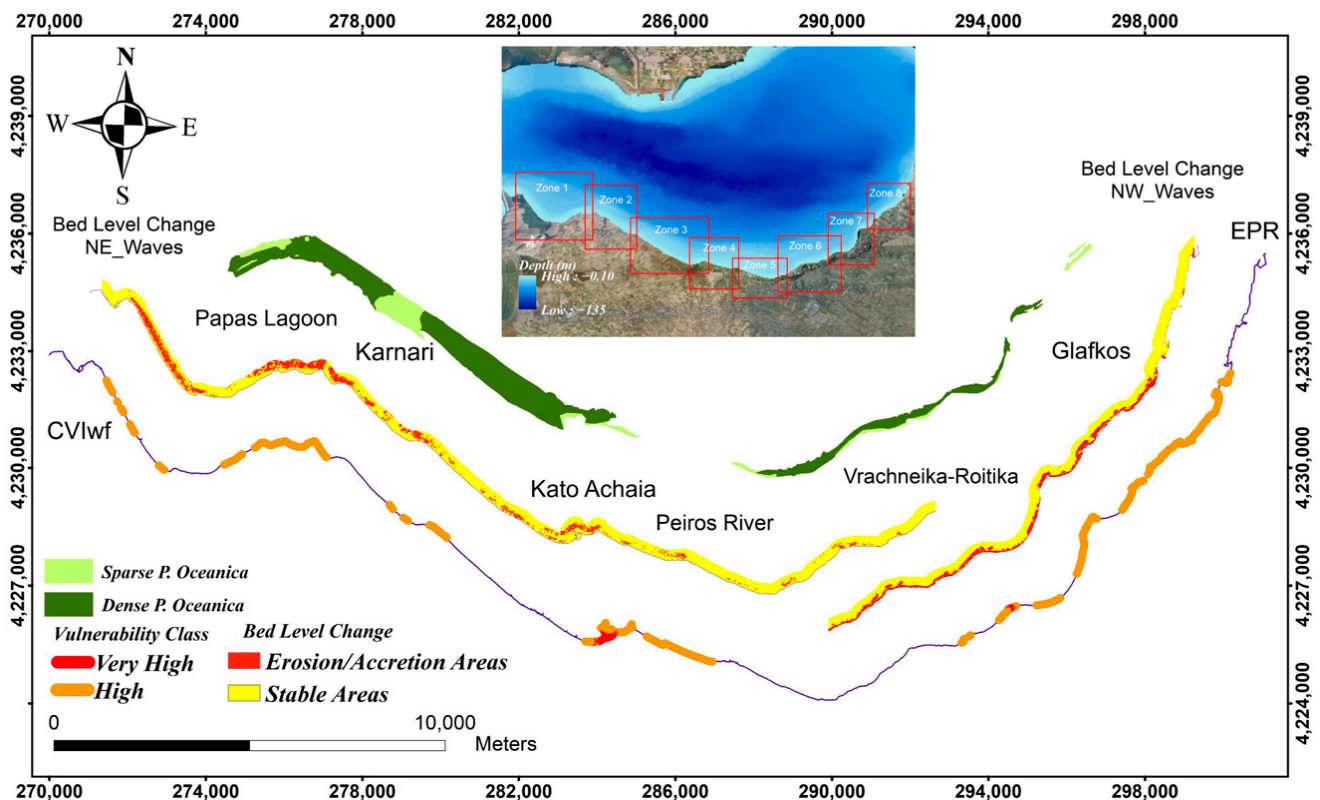
Figure 17. Spatial distribution of high and very high vulnerability classes using CVI$_{WF}$ compared with the rate of bed level change (mostly affected by NE winds in the west and NW waves in the east) and the *P. oceanica* spatial distribution along the coastline of the study area.

These findings are in accordance with the results of other studies in Italy, using CVI that have incorporated the *P. oceanica* vegetation parameter [80,81]. More specifically, the *P. oceanica* parameter was evaluated considering its presence/absence [80] and bottom coverage [81]. The CVI incorporating meadow bottom coverage showed that the absence of meadows is related with the highest vulnerability score, while high, medium, low, and very low vulnerability values are assigned using coverage percentages <25%, 50–25%, 75–50%, and >75%, respectively [81].

6. Conclusions

All the surveying methods presented in the current research proved to be important and necessary for the coastal erosion identification along the coastline of the study area.

In detail, from the performed geotechnical investigations, eight (8) distinguished engineering-geological units were recognized along the coastal zone of the research area. Moreover, the coastal deposits (Sd) were further distinguished in order to provide all the fundamental data for the already discussed hydrodynamic model and the relevant CVI$_{WF}$ calculations.

Using satellite and aerial photo imaging and the DSAS extensions of ArcGIS, such as the NSM and the EPR, the rate of erosion regime along the littoral zone of the study area was estimated through the period 1987–2018. It emerged that the mean rate of change along the coastline is −0.21 m/y, while its largest part (56%) is in a state of low erosion, and 21% in a state of high erosion.

Based on the bathymetric data and the seabed slope gradient, the seafloor in the survey area was separated into five subareas, with the easternmost (a and b) and westernmost (e) subareas characterized by high slope degrees (10°) between the 5 and 15 m isobaths. In addition, *P. oceanica* meadows were identified covering areas of approximately 10 km^2 (42% of the survey area). In general, *P. oceanica* seagrass seems to be becoming much more

extensive to the west of Kato Achaia promontory (zones 1, 2, and 3) due to: (i) having lower slopes and (ii) being further from any anthropogenic interference, such as industrial and recreational coastal activities and urban waste treatments.

Concerning the importance of some parameters such as sea bed level change and *P. oceanica* vegetation in relation to the CVI_{WF} calculations it seems that they coincide better in a high or very high vulnerability regime. For instance, sea bed level change with high rate of erosion/accretion matches with areas of high or very high vulnerability. On the other hand, in the absence of *P. oceanica* vegetation, matches occur with areas of high or very high vulnerability only in the eastern part of the study area in which NW waves are dominant and human population and activities are extensive.

The question of which method or parameter is more important than the other is still under investigation and needs continuous research and measurements. For this reason, a coastal observatory was finally established in the model area (Gulf of Patras) under the framework of the TRITON project. Its purpose is to continually feed the observatory's database with all necessary data (wave height, tidal range, wind direction and intensity, etc.) for further processing and numerical modelling.

At this point, these real-time data may be used at any time to directly update the GIS dataset, the hydrodynamic (numerical) model, and the CVI calculations in the entire investigation area. In terms of the remote sensing surveys, the marine surveys, and partially the geotechnical surveys, they should be repeated at regular intervals because the seabed bathymetry and morphology and the shoreline are very sensitive to any weather changes. Similar approaches have been used in order to collect, rationalize, and mutualize valuable acquired and shared data regarding the coastal risks [23]. Moreover, repeated (4D) remote, marine, and geotechnical surveys could be effective for monitoring coastal areas, allowing the evaluation of the key parameters controlling the complex dynamics of the coastal environment [82].

It may be concluded that regional observatories provide high-precision data that may be used to strengthen the scientific knowledge, develop strategic tools and respond to the public requirement for a better management in the coastal zones.

Author Contributions: Conceptualization, N.D.; methodology, N.D., A.D., K.N., G.P. and N.S.; software, D.A., V.B., D.C., E.F., G.L. and A.M.; validation, N.D., A.D., K.N. and G.P.; formal analysis, N.D., D.A., V.B., D.C., E.F., A.M. and G.L.; investigation, N.D., D.A., V.B., D.C., A.D., E.F., G.L., K.N., G.P. and N.S.; resources, N.D., A.D., K.N., G.P. and N.S.; data curation, N.D., A.D., K.N. and G.P.; writing—original draft preparation, N.D., D.A., V.B., D.C., A.D., E.F., G.L., K.N. and G.P.; writing—review and editing, N.D. and V.B.; visualization, N.D.; supervision, N.D.; project administration, N.D. and N.S. All authors have read and agreed to the published version of the manuscript.

Data Availability Statement: Data are available from the authors upon request.

Conflicts of Interest: The authors declare no conflict of interest.

References

1. IPCC. *Global Warming of 1.5 °C*; IPCC: Geneva, Switzerland, 2018; ISBN 9781009157940.
2. Bunce, M.; Brown, K.; Rosendo, S. Policy Misfits, Climate Change and Cross-Scale Vulnerability in Coastal Africa: How Development Projects Undermine Resilience. *Environ. Sci. Policy* **2010**, *13*, 485–497. [CrossRef]
3. Ferro-Azcona, H.; Espinoza-Tenorio, A.; Calderón-Contreras, R.; Ramenzoni, V.C.; País, M.D.L.M.G.; Mesa-Jurado, M.A. Adaptive Capacity and Social-Ecological Resilience of Coastal Areas: A Systematic Review. *Ocean Coast. Manag.* **2019**, *173*, 36–51. [CrossRef]
4. IPCC. *Climate Change 2014 Part A: Global and Sectoral Aspects*; IPCC: Geneva, Switzerland, 2014; ISBN 9781107641655.
5. Carson, M.; Köhl, A.; Stammer, D.; ASlangen, A.B.; Katsman, C.A.; van de Wal, R.S.W.; Church, J.; White, N. Coastal Sea Level Changes, Observed and Projected during the 20th and 21st Century. *Clim. Chang.* **2016**, *134*, 269–281. [CrossRef]

6. van Dongeren, A.; Ciavola, P.; Martinez, G.; Viavattene, C.; Bogaard, T.; Ferreira, O.; Higgins, R.; McCall, R. Introduction to RISC-KIT: Resilience-Increasing Strategies for Coasts. *Coast. Eng.* **2018**, *134*, 2–9. [CrossRef]

7. Gibbs, M.T. Consistency in Coastal Climate Adaption Planning in Australia and the Importance of Understanding Local Political Barriers to Implementation. *Ocean Coast. Manag.* **2019**, *173*, 131–138. [CrossRef]

8. Ramieri, E.; Hartley, A.J.; Barbanti, A.; Santos, F.D.; Gomes, A.; Hilden, M.; Laihonen, P.; Marinova, N.; Santini, M. Methods for Assessing Coastal Vulnerability to Climate Change. *Eur. Environ. Agency Eur. Top. Cent. Clim. Chang. Impacts Vulnerability Adapt.* **2011**, 1–93.

9. Losada, I.J.; Toimil, A.; Muñoz, A.; Garcia-Fletcher, A.P.; Diaz-Simal, P. A Planning Strategy for the Adaptation of Coastal Areas to Climate Change: The Spanish Case. *Ocean Coast. Manag.* **2019**, *182*, 104983. [CrossRef]

10. Toimil, A.; Losada, I.J.; Nicholls, R.J.; Dalrymple, R.A.; Stive, M.J.F. Addressing the Challenges of Climate Change Risks and Adaptation in Coastal Areas: A Review. *Coast. Eng.* **2020**, *156*, 103611. [CrossRef]

11. Bongarts Lebbe, T.; Rey-Valette, H.; Chaumillon, É.; Camus, G.; Almar, R.; Cazenave, A.; Claudet, J.; Rocle, N.; Meur-Férec, C.; Viard, F.; et al. Designing Coastal Adaptation Strategies to Tackle Sea Level Rise. *Front. Mar. Sci.* **2021**, *8*, 1640. [CrossRef]

12. Gornitz, V. Global Coastal Hazards from Future Sea Level Rise. *Palaeogeogr. Palaeoclimatol. Palaeoecol.* **1991**, *89*, 379–398. [CrossRef]

13. De Serio, F.; Armenio, E.; Mossa, M.; Petrillo, A.F. How to Define Priorities in Coastal Vulnerability Assessment. *Geosciences* **2018**, *8*, 415. [CrossRef]

14. Furlan, E.; Pozza, P.D.; Michetti, M.; Torresan, S.; Critto, A.; Marcomini, A. Development of a Multi-Dimensional Coastal Vulnerability Index: Assessing Vulnerability to Inundation Scenarios in the Italian Coast. *Sci. Total Environ.* **2021**, *772*, 144650. [CrossRef] [PubMed]

15. Hinkel, J.; Klein, R.J.T. Integrating Knowledge to Assess Coastal Vulnerability to Sea-Level Rise: The Development of the DIVA Tool. *Glob. Environ. Chang.* **2009**, *19*, 384–395. [CrossRef]

16. Torresan, S.; Zabeo, A.; Rizzi, J.; Critto, A.; Pizzol, L.; Giove, S.; Marcomini, A. Risk Assessment and Decision Support Tools for the Integrated Evaluation of Climate Change Impacts on Coastal Zones. In Proceedings of the 5th International Congress on Environmental Modelling and Software, Ottawa, ON, Canada, 5–8 July 2010; Volume 3, pp. 2409–2416.

17. Zanuttigh, B.; Simcic, D.; Bagli, S.; Bozzeda, F.; Pietrantoni, L.; Zagonari, F.; Hoggart, S.; Nicholls, R.J. THESEUS Decision Support System for Coastal Risk Management. *Coast. Eng.* **2014**, *87*, 218–239. [CrossRef]

18. Zennaro, F.; Furlan, E.; Simeoni, C.; Torresan, S.; Aslan, S.; Critto, A.; Marcomini, A. Exploring Machine Learning Potential for Climate Change Risk Assessment. *Earth-Sci. Rev.* **2021**, *220*, 103752. [CrossRef]

19. Harris, R.; Furlan, E.; Pham, H.V.; Torresan, S.; Mysiak, J.; Critto, A. A Bayesian Network Approach for Multi-Sectoral Flood Damage Assessment and Multi-Scenario Analysis. *Clim. Risk Manag.* **2022**, *35*, 100410. [CrossRef]

20. Barco, D.; Pham, H.V.; Fogarin, S.; Zanetti, M.; Harris, R.; Rubinetti, S.; Rubino, A.; Zanchettin, D.; Barbariol, F.; Benetazzo, A.; et al. Evaluating Climate Change and Coastal Erosion Risks on the Venice Coastline: A Machine Learning Approach Supporting Multi-Risk Scenario Analysis. In Proceedings of the EGU General Assembly Conference Abstracts, Vienna, Austria, 3–27 May 2022.

21. Environment Agency. Maritime Local Authorities the Coastal Handbook: A Guide for All Those Working on the Coast. *Environ. Agency Marit. Local Authorities* **2010**, *220*.

22. Becker, A.; Brown, J.; Bricheno, L.; Wolf, J. Guidance Note on the Application of Coastal Monitoring for Small Island Developing States. 2020. Available online: https://www.cmeprogramme.org/sites/cme-programme/files/documents/reports/Becker_et_al_NOC_R&C_74_2020.pdf (accessed on 7 January 2023).

23. Kerguillec, R.; Audère, M.; Baltzer, A.; Debaine, F.; Fattal, P.; Juigner, M.; Launeau, P.; Le Mauff, B.; Luquet, F.; Maanan, M.; et al. Monitoring and Management of Coastal Hazards: Creation of a Regional Observatory of Coastal Erosion and Storm Surges in the Pays de La Loire Region (Atlantic Coast, France). *Ocean Coast. Manag.* **2019**, *181*, 104904. [CrossRef]

24. Bio, A.; Bastos, L.; Granja, H.; Pinho, J.L.S.; Goncalves, J.A.; Henriques, R.; Madeira, S.; Magalhaes, A.; Rodrigues, D. Methods for Coastal Monitoring and Erosion Risk Assessment: Two Portuguese Case Studies. *J. Integr. Coast. Zo. Manag.* **2015**, *15*, 47–63. [CrossRef]

25. Romagnoli, C.; Sistilli, F.; Cantelli, L.; Aguzzi, M.; De Nigris, N.; Morelli, M.; Gaeta, M.G.; Archetti, R. Beach Monitoring and Morphological Response in the Presence of Coastal Defense Strategies at Riccione (Italy). *J. Mar. Sci. Eng.* **2021**, *9*, 851. [CrossRef]

26. Almonacid-Caballer, J.; Sánchez-García, E.; Pardo-Pascual, J.E.; Balaguer-Beser, A.A.; Palomar-Vázquez, J. Evaluation of Annual Mean Shoreline Position Deduced from Landsat Imagery as a Mid-Term Coastal Evolution Indicator. *Mar. Geol.* **2016**, *372*, 79–88. [CrossRef]

27. Almeida, L.P.; Almar, R.; Bergsma, E.W.J.; Berthier, E.; Baptista, P.; Garel, E.; Dada, O.A.; Alves, B. Deriving High Spatial-Resolution Coastal Topography from Sub-Meter Satellite Stereo Imagery. *Remote Sens.* **2019**, *11*, 590. [CrossRef]

28. Hodúl, M.; Bird, S.; Knudby, A.; Chénier, R. Satellite Derived Photogrammetric Bathymetry. *ISPRS J. Photogramm. Remote Sens.* **2018**, *142*, 268–277. [CrossRef]

29. Turner, I.L.; Harley, M.D.; Almar, R.; Bergsma, E.W.J. Satellite Optical Imagery in Coastal Engineering. *Coast. Eng.* **2021**, *167*, 103919. [CrossRef]

30. Brock, J.C.; Purkis, S.J. The Emerging Role of Lidar Remote Sensing in Coastal Research and Resource Management. *J. Coast. Res.* **2009**, *10053*, 1–5. [CrossRef]

31. Young, A.P.; Olsen, M.J.; Driscoll, N.; Rick, R.E.; Gutierrez, R.; Guza, R.T.; Johnstone, E.; Kuester, F. Comparison of Airborne and Terrestrial Lidar Estimates of Seacliff Erosion in Southern California. *Photogramm. Eng. Remote Sensing* **2010**, *76*, 421–427. [CrossRef]

32. Klemas, V. Beach Profiling and LIDAR Bathymetry: An Overview with Case Studies. *J. Coast. Res.* **2011**, *27*, 1019–1028. [CrossRef]

33. O'Dea, A.; Brodie, K.L.; Hartzell, P. Continuous Coastal Monitoring with an Automated Terrestrial Lidar Scanner. *J. Mar. Sci. Eng.* **2019**, *7*, 37. [CrossRef]

34. Nikolakopoulos, K.G.; Lampropoulou, P.; Fakiris, E.; Sardelianos, D.; Papatheodorou, G. Synergistic Use of UAV and USV Data and Petrographic Analyses for the Investigation of Beachrock Formations: A Case Study from Syros Island, Aegean Sea, Greece. *Minerals* **2018**, *8*, 534. [CrossRef]

35. Archetti, R.; Zanuttigh, B. Integrated Monitoring of the Hydro-Morphodynamics of a Beach Protected by Low Crested Detached Breakwaters. *Coast. Eng.* **2010**, *57*, 879–891. [CrossRef]

36. Uunk, L.; Wijnberg, K.M.; Morelissen, R. Automated Mapping of the Intertidal Beach Bathymetry from Video Images. *Coast. Eng.* **2010**, *57*, 461–469. [CrossRef]

37. Almar, R.; Bergsma, E.W.J.; Maisongrande, P.; de Almeida, L.P.M. Wave-Derived Coastal Bathymetry from Satellite Video Imagery: A Showcase with Pleiades Persistent Mode. *Remote Sens. Environ.* **2019**, *231*, 111263. [CrossRef]

38. Apostolopoulos, D.N.; Nikolakopoulos, K.G. Synergy of UAV Data and in Situ Measurements for the Shoreline Mapping in Arkoudi Beach, Western Greece. In *Earth Resources and Environmental Remote Sensing/GIS Applications XIII*; SPIE: Bellingham, WA, USA, 2022; Volume 12268, pp. 244–256. [CrossRef]

39. Nikolakopoulos, K.; Kyriou, A.; Koukouvelas, I.; Zygouri, V.; Apostolopoulos, D. Combination of Aerial, Satellite, and UAV Photogrammetry for Mapping the Diachronic Coastline Evolution: The Case of Lefkada Island. *ISPRS Int. J. Geo-Inf.* **2019**, *8*, 489. [CrossRef]

40. Viaña-Borja, S.P.; Ortega-Sánchez, M. Automatic Methodology to Detect the Coastline from Landsat Images with a New Water Index Assessed on Three Different Spanish Mediterranean Deltas. *Remote Sens.* **2019**, *11*, 2186. [CrossRef]

41. McFeeters, S.K. The Use of the Normalized Difference Water Index (NDWI) in the Delineation of Open Water Features. *Int. J. Remote Sens.* **1996**, *17*, 1425–1432. [CrossRef]

42. Xu, H. Modification of Normalised Difference Water Index (NDWI) to Enhance Open Water Features in Remotely Sensed Imagery. *Int. J. Remote Sens.* **2006**, *27*, 3025–3033. [CrossRef]

43. Feyisa, G.L.; Meilby, H.; Fensholt, R.; Proud, S.R. Automated Water Extraction Index: A New Technique for Surface Water Mapping Using Landsat Imagery. *Remote Sens. Environ.* **2014**, *140*, 23–35. [CrossRef]

44. Baily, B.; Nowell, D. Techniques for Monitoring Coastal Change: A Review and Case Study. *Ocean Coast. Manag.* **1996**, *32*, 85–95. [CrossRef]

45. Boak, E.H.; Turner, I.L. Shoreline Definition and Detection: A Review. *J. Coast. Res.* **2005**, *21*, 688–703. [CrossRef]

46. Apostolopoulos, D.; Nikolakopoulos, K. A Review and Meta-Analysis of Remote Sensing Data, GIS Methods, Materials and Indices Used for Monitoring the Coastline Evolution over the Last Twenty Years. *Eur. J. Remote Sens.* **2021**, *54*, 240–265. [CrossRef]

47. Fakiris, E.; Blondel, P.; Papatheodorou, G.; Christodoulou, D.; Dimas, X.; Georgiou, N.; Kordella, S.; Dimitriadis, C.; Rzhanov, Y.; Geraga, M.; et al. Multi-Frequency, Multi-Sonar Mapping of Shallow Habitats-Efficacy and Management Implications in the National Marine Park of Zakynthos, Greece. *Remote Sens.* **2019**, *11*, 461. [CrossRef]

48. Pasqualini, V.; Pergent-Martini, C.; Pergent, G. Use of Remote Sensing for the Characterization of the Mediterranean Coastal Environment—The Case of Posidonia Oceanica. *J. Coast. Conserv.* **1998**, *4*, 59–66. [CrossRef]

49. Duarte, C.M. Seagrass Depth Limits. *Aquat. Bot.* **1991**, *40*, 363–377. [CrossRef]

50. Terrados, J.; Duarte, C.M. Experimental Evidence of Reduced Particle Resuspension within a Seagrass (*Posidonia Oceanica* L.) Meadow. *J. Exp. Mar. Bio. Ecol.* **2000**, *243*, 45–53. [CrossRef]

51. Boudouresque, C.F.; Meinesz, A. Découverte de l'herbier de Posidonie. *Cah. Parc Nation* **1982**, *4*, 1–79.

52. Albatal, A.; Stark, N.; Castellanos, B. Estimating in Situ Relative Density and Friction Angle of Nearshore Sand from Portable Free-Fall Penetrometer Tests. *Can. Geotech. J.* **2020**, *57*, 17–31. [CrossRef]

53. Boumpoulis, V.; Depountis, N.; Pelekis, P.; Sabatakakis, N. SPT and CPT Application for Liquefaction Evaluation in Greece. *Arab. J. Geosci.* **2021**, *14*, 1631. [CrossRef]

54. Bilici, C.; Stark, N.; Friedrichs, C.T.; Massey, G.M. Coupled Sedimentological and Geotechnical Data Analysis of Surficial Sediment Layer Characteristics in a Tidal Estuary. *Geo-Marine Lett.* **2019**, *39*, 175–189. [CrossRef]

55. Jafari, N.H.; Harris, B.D.; Stark, T.D. Geotechnical Investigations at the Caminada Headlands Beach and Dune in Coastal Louisiana. *Coast. Eng.* **2018**, *142*, 82–94. [CrossRef]

56. Watts, C.W.; Tolhurst, T.J.; Black, K.S.; Whitmore, A.P. In Situ Measurements of Erosion Shear Stress and Geotechnical Shear Strength of the Intertidal Sediments of the Experimental Managed Realignment Scheme at Tollesbury, Essex, UK. *Estuar. Coast. Shelf Sci.* **2003**, *58*, 611–620. [CrossRef]

57. Cao, C.; Sun, Y.; Sun, H.; Song, Y. Erosion Resistance and Scouring Depth of Fine-Grained Seabed of the Huanghe River Estuary, China. *Bull. Eng. Geol. Environ.* **2018**, *77*, 897–910. [CrossRef]

58. Wu, W.; Perera, C.; Smith, J.; Sanchez, A. Critical Shear Stress for Erosion of Sand and Mud Mixtures. *J. Hydraul. Res.* **2018**, *56*, 96–110. [CrossRef]

59. Perera, C.; Smith, J.; Wu, W.; Perkey, D.; Priestas, A. Erosion Rate of Sand and Mud Mixtures. *Int. J. Sediment Res.* **2020**, *35*, 563–575. [CrossRef]

60. Winterwerp, J.C.; van Kesteren, W.G.M.; van Prooijen, B.; Jacobs, W. A Conceptual Framework for Shear Flow–Induced Erosion of Soft Cohesive Sediment Beds. *J. Geophys. Res. Ocean.* **2012**, *117*, 1–17. [CrossRef]

61. Ružić, I.; Jovančević, S.D.; Benac, Č.; Krvavica, N. Assessment of the Coastal Vulnerability Index in an Area of Complex Geological Conditions on the Krk Island, Northeast Adriatic Sea. *Geosciences* **2019**, *9*, 219. [CrossRef]

62. Boumboulis, V.; Apostolopoulos, D.; Depountis, N.; Nikolakopoulos, K. The Importance of Geotechnical Evaluation and Shoreline Evolution in Coastal Vulnerability Index Calculations. *J. Mar. Sci. Eng.* **2021**, *9*, 423. [CrossRef]

63. Marques Machado, F.M.; Gameiro Lopes, A.M.; Ferreira, A.D. Numerical Simulation of Regular Waves: Optimization of a Numerical Wave Tank. *Ocean Eng.* **2018**, *170*, 89–99. [CrossRef]

64. Leftheriotis, G.A.; Chalmoukis, I.A.; Oyarzun, G.; Dimas, A.A. A Hybrid Parallel Numerical Model for Wave-induced Free-surface Flow. *Fluids* **2021**, *6*, 350. [CrossRef]

65. Pikelj, K.; Ružić, I.; Ilić, S.; James, M.R.; Kordić, B. Implementing an Efficient Beach Erosion Monitoring System for Coastal Management in Croatia. *Ocean Coast. Manag.* **2018**, *156*, 223–238. [CrossRef]

66. Harley, M.D.; Ciavola, P. Managing Local Coastal Inundation Risk Using Real-Time Forecasts and Artificial Dune Placements. *Coast. Eng.* **2013**, *77*, 77–90. [CrossRef]

67. O'Reilly, W.C.; Olfe, C.B.; Thomas, J.; Seymour, R.J.; Guza, R.T. The California Coastal Wave Monitoring and Prediction System. *Coast. Eng.* **2016**, *116*, 118–132. [CrossRef]

68. Valchev, N.; Eftimova, P.; Andreeva, N. Implementation and Validation of a Multi-Domain Coastal Hazard Forecasting System in an Open Bay. *Coast. Eng.* **2018**, *134*, 212–228. [CrossRef]

69. Apostolopoulos, D.N.; Nikolakopoulos, K.G. Identifying Sandy Sites under Erosion Regime along the Prefecture of Achaia, Using Remote Sensing Techniques. *J. Appl. Remote Sens.* **2022**, *17*, 022206. [CrossRef]

70. Moore, L.J. Shoreline Mapping Techniques. *J. Coast. Res.* **2000**, *16*, 111–124.

71. Byrnes, M.R.; Anders, F.J. Accuracy of Shoreline Change Rates as Determined From Maps and Aerial Photographs. *Shore Beach Obs.* **1991**, *58*, 30.

72. Apostolopoulos, D.N.; Nikolakopoulos, K.G. Assessment and Quantification of the Accuracy of Low-and High-Resolution Remote Sensing Data for Shoreline Monitoring. *ISPRS Int. J. Geo-Inf.* **2020**, *9*, 391. [CrossRef]

73. Apostolopoulos, D.N.; Nikolakopoulos, K.G. Statistical Methods to Estimate the Accuracy of Diachronic Low-Resolution Satellite Instruments for Shoreline Monitoring. *J. Appl. Remote Sens.* **2021**, *16*, 012007. [CrossRef]

74. Hiller, R.; Calder, B.R.; Hogarth, P.; Gee, L. Adapting CUBE for Phase Measuring Bathymetric Sonars. In Proceedings of the International Conference on High-Resolution Survey in Shallow Water, Plymouth, Devon, UK, 12–15 September 2005.

75. Blondel, P. *The Handbook of Sidescan Sonar*; Springer Science & Business Media: Berlin, Germany, 2009; ISBN 9783540426417.

76. *Software Flow Model FM, Reference Mannual*, DHI MIKE 21; DHI GRAS A/S Agern Allé 5 2970: Hørsholm, Danmark, 2014.

77. *Software Spectral Waves FM Module, User Guide*, DHI MIKE 21 SW; DHI GRAS A/S Agern Allé 5 2970: Hørsholm, Danmark, 2014.

78. Battjes, J.A.; Janssen, J.P.F.M. Energy loss and set-up due to breaking of random waves. *Coast. Eng.* **1978**, 569–587.

79. Smagorisky, J. General circulation experiments with the primitive equations. *Mon. Weather Rev.* **1963**, *91*, 99–164. [CrossRef]

80. Pantusa, D.; D'Alessandro, F.; Riefolo, L.; Principato, F.; Tomasicchio, G.R. Application of a Coastal Vulnerability Index. A Case Study along the Apulian Coastline, Italy. *Water (Switz.)* **2018**, *10*, 1218. [CrossRef]

81. Pantusa, D.; D'Alessandro, F.; Frega, F.; Francone, A.; Tomasicchio, G.R. Improvement of a Coastal Vulnerability Index and Its Application along the Calabria Coastline, Italy. *Sci. Rep.* **2022**, *12*, 21959. [CrossRef] [PubMed]

82. Stanghellini, G.; Bidini, C.; Romagnoli, C.; Archetti, R.; Ponti, M.; Turicchia, E.; Del Bianco, F.; Mercorella, A.; Polonia, A.; Giorgetti, G.; et al. Repeated (4D) Marine Geophysical Surveys as a Tool for Studying the Coastal Environment and Ground-Truthing Remote-Sensing Observations and Modeling. *Remote Sens.* **2022**, *14*, 5901. [CrossRef]